Symmetry-Based Pulse Sequences in Solid–State NMR and Applications to Biological Systems

Xin Zhao, Marina Carravetta, P.K.Madhu, and Malcolm H.Levitt

March 18, 2003

[†]Department of Chemistry, University of Southampton, Southampton SO17 1BJ , UK

[⋆]Author to whom correspondence should be addressed at: mhl@soton.ac.uk

Abstract

We present some applications of solid–state nuclear magnetic resonance to model compounds and biological systems. We highlight a class of pulse sequences that are designed based on symmetry properties of the internal spin interactions. Examples are given showing resonance assignments, determination of internuclear distances, and torsion angle determinations in representative model systems as well as true biological systems.

1 Introduction

The use of solution–state nuclear magnetic resonance (NMR) for determining the high–resolution structure of biomolecules is well established. However there are many systems which are not amenable to solution–state NMR, because they do not dissolve easily or because they have slow molecular motion in solution. Many membrane proteins belong to this class. Their study may greatly benefit from the application of solid–state NMR.

In solid–state NMR, all the spin interactions survive motional averaging, unlike the case of solution–state NMR where all interactions except the isotropic scalar coupling, J, and isotropic chemical shift average to zero due to the molecular Brownian motion [1]. The spin interactions present in the solid–state NMR of spin—-$\frac{1}{2}$ systems are the isotropic and anisotropic parts of the scalar coupling, the chemical shift, and the dipolar coupling both homonuclear (between like spins) and heteronuclear (between unlike spins). These interactions provide a wealth of structural and dynamic information. For example, estimation of dipolar couplings between nuclei allows internuclear distance measurements. Measurement of chemical shift anisotropy (CSA) provides information about the local electronic environment and molecular geometry [1].

The many anisotropic spin interactions, though useful, typically lead to resolution and sensitivity problems. For instance, solid–state ^{1}H NMR is

generally quite difficult since the homonuclear dipolar couplings are of the order of tens of kHz, leading to broad spectral peaks. The nuclei that can be observed most easily in the solid state are low-γ species that do not have strong homonuclear couplings. Nuclei that fall into this class are ^{13}C and ^{15}N. In biological solid–state NMR, the abundance of such nuclei is usually enhanced by isotopic labelling. This is done either by chemical synthesis or by isolating biomolecules from organisms grown in a labelled medium.

In this review, the "high-γ" species (typically protons) is denoted I, while the "low-γ" species (typically ^{13}C or ^{15}N) is denoted S.

Resolution and sensitivity enhancement in solid–state NMR are often achieved by three means: magic angle spinning (MAS), heteronuclear dipolar decoupling by the use of radiofrequency (rf) fields and transfer of polarisation from the high-γ spins to the low-γ spins via cross–polarisation (CP) [1]. These techniques give well resolved spectral lines for the low-γ spins but suppress the anisotropic interactions. This leads to a loss of geometry information.

Recoupling schemes have been devised to selectively retrieve the geometry information lost by the use of the decoupling methods [1–3]. These sequences aim to recouple the CSA, homonuclear or heteronuclear dipolar couplings selectively, thereby allowing the measurement of structurally important geometry parameters, without loss of spectral sensitivity and resolution.

In this review a brief outline will be given of some common recoupling methods, together with some relevant applications. We highlight a procedure for systematically developing recoupling sequences based on symmetry properties of the internal spin interactions. This approach yields solutions which depend on the type of interaction that needs to be recoupled. Selected applications and spectra will be shown. We avoid detailed mathematical description, giving instead appropriate references where required. A more extensive review of many of the theoretical and practical aspects of sequences based on symmetry has appeared [4].

2 MAS, Decoupling and CP

As stated in the Introduction, nuclear spins that do not experience strong homonuclear dipolar couplings are the most suitable candidates for observation in solid–state NMR. However, many such spins experience large CSA interactions and hence still provide poor resolution in powders. A method for averaging out such anisotropies is called magic–angle spinning (MAS) [5,6]. In MAS the sample is spun at an angle of $\tan^{-1}\sqrt{2} \approx 54.7^{\rm o}$ with respect to the magnetic field, as shown in Fig. 1a. Currently, the maximum available spinning frequency is about 50 kHz [**?**]. MAS leads to a zero time average of those spin interactions which transform as second-rank spherical tensors under spatial rotations. This includes the CSA and the through-space dipole-dipole interactions.

In most cases, MAS alone does not remove the effects of heteronuclear dipolar couplings. It must be augmented by applying an rf field, either continuous or modulated in phase or amplitude, at the Larmor frequency of the high-γ spins [1]. A schematic of this is shown in Fig. 1b. Several decoupling schemes have been introduced. The two popular ones in vogue are continuous–wave, CW, decoupling and two–pulse phase–modulated (TPPM) decoupling [7]. In TPPM decoupling a train of pulses pairs with flip angles close to $180^{\rm o}$ and phases $\pm\phi$ and $\phi \approx 10\,{\rm deg}$ is applied. Both the flip–angle and phase of the pulses need to be carefully optimised for good performance. Recently, a variety of other methods has appeared [**?**], such as XiX [8] and DROOPY [**?**].

A further increase in the signal strength of the low-γ species is provided by the elegant technique of cross–polarisation (CP) which transfers magnetisation from the high-γ spins to the low-γ spins [9]. This involves simultaneous application of two rf fields, one at the Larmor frequency of the high-γ spins and one at the Larmor frequency of the low-γ spins, such that the nutation frequencies of the two spin species under the rf fields are the same [11]. For spins–$\frac{1}{2}$ the nutation frequency is given by $\omega_{nut} = |\frac{1}{2}\gamma B_{rf}^{peak}|$ where γ

is the nuclear gyromagnetic ratio and B_{rf}^{peak} the peak transverse rf field in the coil [10]. Efficient magnetisation transfer usually takes place around the condition, $\omega_{nut}^{I} = \omega_{nut}^{S}$, called the Hartmann–Hahn condition [11]. This typically leads to a maximum S spin signal enhancement approaching the value γ_I/γ_S, which is about 4 for the case $I =^{1}$H, $S =^{13}$C. In addition, low-γ spins often have much longer relaxation times, T_1, than high-γ and hence require longer recycle delays if they are observed directly. Under CP, since the magnetisation originates from the high-γ species, shorter recycle delays are possible, which speeds up the experiments. A schematic CP pulse sequence is shown in Fig. 1c. Variants of CP schemes have been introduced that significantly enhance the CP efficiency particularly under high MAS frequencies. The most commonly used scheme is ramped–amplitude CP, where the rf field on one of the channels is gradually changed to cover a range of nutation frequencies [12].

In the presence of heteronuclear decoupling of the abundant spins, fast MAS leads to spectra of the low-γ species with peaks at the isotropic chemical shift values. In practice, a good averaging of CSA takes place even when the MAS frequencies are less than the strength of the CSA. In this case the static powder shape breaks up into a set of sidebands spaced by the spinning frequency and centered at the isotropic shift frequency. As the MAS frequency increases the sidebands move outwards with diminishing intensity, and the centrebands grow in intensity. This scenario is depicted in Fig. 2. Spectrum (a) shows the ^{1}H–decoupled CSA broadened powder pattern of the $^{13}CH_2$ and ^{13}CO peaks in a uniformly ^{13}C–labelled glycine sample. Spectra (b–d) show the effect of MAS on this static powder envelope.

The combination of CP and MAS, called CPMAS, is used routinely for the observation of rare spins [13]. The spectra in Fig. 2 were all acquired by employing MAS, decoupling and CP except Fig. 2a which was acquired under static condition with CP and decoupling.

3 Internal Spin Hamiltonians

In a spin–$\frac{1}{2}$ system the following spin interactions are present: J– couplings, CSA, homonuclear and heteronuclear dipolar couplings. In general these interactions are tensors with both a spatial part and spin part [14]. The spatial part expresses the dependence of the interaction on the molecular orientations, keeping the spin polarisations and the static magnetic field fixed. It may be manipulated by MAS. The spin part expresses the dependence of the interaction on the spin orientations, keeping the molecular orientation and the static magnetic field fixed. It may be manipulated by the application of a rf field. The spatial part of dipolar interactions is directly related to the geometry in the form of distances and angles.

The Hamiltonian of a spin system in solid–state NMR may be written as

$$\mathcal{H} = \mathcal{H}_{int} + \mathcal{H}_{ext} \tag{1}$$

where $\mathcal{H}_{int}$ corresponds to the interactions of the spins with each other and to the molecular environment, $\mathcal{H}_{ext}$ corresponds to couplings between the nuclear spins and the applied magnetic fields.

The external interactions are the Zeeman interaction with the large static magnetic field, $\mathcal{H}_Z$, which is often the most dominant interaction, and with the applied rf field, $\mathcal{H}_{rf}$. Hence,

$$\mathcal{H}_{ext} = \mathcal{H}_Z + \mathcal{H}_{rf} \tag{2}$$

The internal spin Hamiltonian may be written as

$$\mathcal{H}_{int} = \mathcal{H}_J + \mathcal{H}_{CSA} + \mathcal{H}_{DD}^{homo} + \mathcal{H}_{DD}^{hetero} \tag{3}$$

where $\mathcal{H}_J$ corresponds to the J–coupling, $\mathcal{H}_{CSA}$ corresponds to the chemical shift anisotropy, $\mathcal{H}_{DD}^{homo}$ corresponds to the homonuclear dipolar coupling and $\mathcal{H}_{DD}^{hetero}$ corresponds to the heteronuclear dipolar coupling. These terms may be written as sums over all spin pais:

$$\mathcal{H}_{DD}^{homo} = \sum_{j<k,homo} \mathcal{H}_{DD}^{jk}$$

$$\mathcal{H}_{DD}^{hetero} = \sum_{j<k,hetero} \mathcal{H}_{DD}^{jk} \tag{4}$$

Invoking the secular approximation (*i.e* only retaining those terms of the internal Hamiltonian that commute with the predominant Zeeman Hamiltonian), the homonuclear coupling $\mathcal{H}_{DD}^{jk}$ and $\mathcal{H}_{DD}^{IS}$ may be expressed as [14]

$$\begin{aligned} \mathcal{H}_{DD}^{jk} &= \frac{b}{2}(3cos^2\theta_{jk} - 1)(3I_{jz}I_{kz} - I_j \cdot I_k) \\ \mathcal{H}_{DD}^{hetero} &= b(3cos^2\theta_{IS} - 1)I_z S_z \\ b &= -\frac{\mu_0}{4\pi}\hbar\frac{1}{r^3}\gamma_I\gamma_S \end{aligned} \tag{5}$$

where r is the distance between the spins. In the homonuclear case, θ_{jk} is the angle subtended by the dipolar vector joining the spins I_j and I_k with respect to the external magnetic field. θ_{IS} is the angle subtended by the vector joining the I and S with respect to the external magnetic field in the heteronuclear case. A measurement of these interactions leads directly to structural information.

4 Recoupling Techniques in Solid–State NMR

CPMAS, though helpful in giving high–resolution isotropic spectral lines, suppresses the effect of the anisotropic interactions and largely removes the geometry information from the spectrum. Retrieving this information has been one of the major concerns in solid–state NMR. Sequences that do this are called recoupling sequences. These recoupling sequences reintroduce the anisotropic interactions for certain time periods during MAS .

A general schematic of the recoupling strategy may be understood with reference to Fig. 3. Figure 3a shows the modulation of a heteronuclear interaction under MAS. The time average of the interaction is equal to zero. The averaging-out of the interaction can be prevented by applying, for instance, two π pulses in a rotor period as shown in Fig. 3b. The time average of the interactions does not vanish anymore, but will be present although scaled by a certain factor depending upon the pulse sequence, called the

scaling factor, κ [1–3]. The scenario in Fig. 3 applies to the recoupling of heteronuclear dipolar interactions in the popular rotational echo double resonance (REDOR) method [22, 23].

Any recoupling scheme involves an interplay of both MAS and rf irradiation. The first true recoupling sequence involved recoupling of the CSA by applying a repetitive pulse train synchronous with the sample rotation [16] followed by rotary resonance recoupling (R^3) [20] and REDOR [22, 23] involving heteronuclear dipolar recoupling, and rotational resonance [17–19] involving homonuclear dipolar recoupling.

A variety of recoupling sequences has been introduced since then, including dipolar recoupling at the magic–angle (DRAMA) [24, 25], radio–frequency driven recoupling (RFDR) [26–28], double–quantum homonuclear rotary resonance (HORROR) [29] and DRAWS [**?**]. A good summary of many of these recoupling sequences may be found in Ref. [2, 3].

In most cases, a recoupling sequence should be insensitive to imperfection in the phases and amplitudes of the rf pulses and rf inhomogeneity, should be sufficiently broad–banded to cover a wide range of chemical shift differences, and should be able to selectively discriminate various internal spin interactions. In the following sections, a systematic theory is described which leads to a systematic design of recoupling sequences based on the symmetry of the internal spin Hamiltonians [4, 30]. This approach was first used explicitly in the design of the C7 pulse sequence [33] and has since been used for the construction of a wide variety of experiments. Some of these are discussed further below.

5 Symmetry Properties of the Spin Interactions

The spin interactions in NMR have well defined transformation properties under rotation. Three types of rotation are involved, in general. They are, rotations of the molecular framework (space), rotations of the nuclear spin polarisation (spin) and rotations of the external magnetic field. The

transformation properties of a spin interaction under these rotations is characterised by its set of rotational ranks.

Characterisation of an internal Hamiltonian may be done based on the quantum numbers of the space and spin part. The space rank of a spin interaction is denoted as l and spin rank as λ. An irreducible spherical tensor of rank l has $2l+1$ components taking values from $m = -l, -l+1, \cdots +l$. A spatial rotation, such as MAS, induces a mixing of the $(2l+1)$ space components. Similarly, the spin rank λ has $(2\lambda+1)$ components taking values $\mu = -\lambda, -\lambda+1, \cdots +\lambda$. A spin rotation in the interaction frame of the rf field induces a mixing of the $(2\lambda+1)$ spin components.

Each interaction can therefore be regarded as a superposition of $(2l+1) \times (2\lambda+1)$ components in the presence of sample rotation (MAS) and resonant rf fields. A particular spin interaction, $\mathcal{H}^{\Lambda}$ may be written as

$$\mathcal{H}^{\Lambda} = \sum_{m=-l}^{+l} \sum_{\mu=-\lambda}^{+\lambda} \mathcal{H}^{\Lambda}_{lm\lambda\mu} \tag{6}$$

In the case of exact MAS, the components with $l = 2$ and $m = 0$ vanish [4]. Expressions for $\mathcal{H}^{\Lambda}$ may be found in Ref. [31, 32]. Table 1 gives the ranks for the most important spin interactions and shows that a distinction may be made among the spin interactions depending on their space and/or spin ranks. Selective recoupling of these interactions is possible by designing pulse sequences based on their transformation properties.

6 Symmetry–Based Recoupling Sequences

There are two large classes of pulse sequences based on symmetry principles. These are known as CN^{ν}_{n} and RN^{ν}_{n} sequences [4].

Both CN^{ν}_{n} and RN^{ν}_{n} sequences are characterised by three symmetry numbers, N, n and ν. N is called the step number, while n and ν are called the spin and space winding numbers. The values of these symmetry numbers define selection rules which indicate which interactions are decoupled or recoupled to first order in average Hamiltonian theory [33, 34].

6.1 CN_n^ν Sequences

A CN_n^ν sequence may be constructed by dividing n rotational periods of the sample into N equal intervals. During each of these intervals a rf pulse sequence is applied which is cyclic, in the sense that it induces a rotation of the nuclear spins through an integer multiple of 360°. The winding number ν defines the phase difference between successive rf cycles, which is given by $2\pi\nu/N$. The sample hence rotates (in space, MAS) through n full rotations and simultaneously experiences a set of rf pulses, the phases of which advance through ν full rotations. A schematic timing diagram is shown in Fig. 4.

The following selection rule determines whether a spin interaction is symmetry–allowed to first order, under a CN_n^ν sequence:

$$\bar{\mathcal{H}}^{(1)}_{lm\lambda\nu} = 0 \qquad \text{if } mn - \mu\lambda \neq NZ \tag{7}$$

where Z denotes any integer [31, 33, 35]. The superscript (1) indicates that the selection rule is valid only to first–order in average Hamiltonian theory [4].

For illustration, consider a pulse sequence with symmetry $C7_2^1$, i.e., $N = 7$, $n = 2$ and $\nu = 1$. Consider a double–quantum dipole-dipole term with $\{l, m, \lambda, \mu\} = \{2, 1, 2, 2\}$. The expression $mn - \mu\nu$ yields a value 0, which is an integer multiple of N=7, and hence this term is symmetry-allowed under the pulse sequence $C7_2^1$. Consider the case of a CSA term with $\{l, m, \lambda, \mu\} = \{2, 2, 1, 1\}$. The expression $mn - \mu\nu$ yields a value 5 which is not a multiple of $N = 7$. Hence this CSA interaction is symmetry-forbidden under $C7_2^1$. This calculation may be repeated for all CSA terms with $l = 2$ and $\lambda = 1$. They are all symmetry forbidden under $C7_2^1$.

It is possible to depict the selection rules by a space–spin selection diagram, as shown in Fig. 5. In the case of $C7_2^1$, all CSA terms are suppressed while two homonuclear DD coupling terms and one isotropic chemical–shift term are allowed. This sequence therefore recouples homonuclear DD coupling terms and is compensated for the effects of CSA, to first order. Since

only dipole-dipole terms with spin quantum number $\mu = \pm 2$ are allowed, this symmetry generates a CSA–compensated double–quantum recoupling sequence [4].

6.2 RN_n^ν Sequences

The general strategy for designing sequences of the form RN_n^ν is as follows [4]:

- Select a pulse sequence element R that rotates resonant spins by 180^o around the x–axis. This element may be a single π pulse, a composite π pulse, or a smoothly modulated rf pulse.
- Derive the pulse sequence element R' by changing the sign of all rf phases in the element R.
- Choose the rf field amplitude such that the duration of R and R', denoted by τ_R, is equal to $\tau_R = n\tau_r/N$, where $\tau_r = 2\pi/\omega_r$ is the rotor period, N is an even integer, and n is any integer. Here ω_r is the angular spinning frequency.
- Form the sequence RN_n^ν by concatenating $N/2$ phase shifted $\{R, R'\}$ pairs as follows:

$$\begin{aligned} RN_n^\nu &= (R)_\phi (R')_{-\phi} (R)_\phi (R')_{-\phi} \cdots (R')_{-\phi} \\ &\equiv \{R_\phi R'_{-\phi}\}^{N/2} \end{aligned}$$

  where the extra phase shifts are specified by $\phi = \pi\nu/N$, and ν is an integer.

A schematic of the construction of a RN_n^ν sequence is shown in Fig. 6.

The entire sequence RN_n^ν consists of $N/2$ contiguous RR' pairs spanning n rotational periods.

The selection rule for RN_n^ν sequences is as follows:

$$\bar{\mathcal{H}}^{(1)}_{lm\lambda\nu} = 0 \qquad \text{if } mn - \mu\lambda \neq \tfrac{N}{2} Z_\lambda \tag{8}$$

Z_λ denotes any integer with the same parity as λ. If λ is odd, then Z_λ is any odd integer; if λ is even, then Z_λ is any even integer [32, 34]. This selection rule is more restrictive than the selection rules for CN_n^ν sequences [4].

For illustration, consider a pulse sequence with symmetry $R18_2^5$. Consider CSA and heteronuclear DD interactions both of which have $\{l, \lambda\} = \{2, 1\}$. Since l=2, there are four m components with $m = (-2, -1, +1, +2)$. Since λ=1, there are three μ components with $\mu = (-1, 0, +1)$. The selection rule $mn - \mu\nu$ yields 9 and -9 for the combinations $\{l, m, \lambda, \mu\}$=$\{2, 2, 1, -1\}$ and $\{2, -2, 1, 1\}$. These terms are both symmetry-allowed since 9 is an odd integer multiple of $\frac{N}{2} = 9$, and the spin rank λ is also odd. Consider now homonuclear DD and isotropic chemical shift terms. For the homonuclear DD interaction, $l = 2$ and $\lambda = 2$. No combination of $\{l, m, \lambda, \mu\}$ yields an even integer multiple of $\frac{N}{2} = 9$ since the spin rank λ is even. This means that homonuclear DD interaction are symmetry forbidden for the $R18_2^5$ sequence. The same holds good for isotropic chemical shift terms where $l = 0$ and λ=1. Hence, a $R18_2^5$ sequence is a suitable candidate for recoupling heteronuclear DD interactions in the presence of homonuclear DD interactions, or for measuring CSA in systems with strong homonuclear DD interactions [36].

Fig. 7 illustrates diagrammatically the selection rule for $R18_2^5$. CSA and heteronuclear DD terms are symmetry–allowed while homonuclear DD coupling terms and isotropic chemical–shift terms are symmetry–forbidden.

7 Applications of Symmetry-Based Sequences

Solid–state NMR is now used for investigating the molecular structure of many biologically interesting systems, such as fibrils, fibres, membrane proteins and enzyme proteins. Some examples are given in Ref. [37–42]. In the following section, we concentrate on a few applications of the symmetry-based sequences to biological systems. A systematic investigation of any biological system requires the following: sequential assignments via through–bond (scalar couplings) or through–space (dipolar couplings), homonuclear

and heteronuclear distance measurements, and torsion angle measurements. This information can shed light on other mechanistic features like hydrogen bonds and dynamic effects.

7.1 Assignment Techniques

The route to structure determination of biomolecules is well established in solution–state NMR. The starting point in spectral analysis is the assignment of the spectral peaks to the respective amino acids. We first discuss the application of symmetry–based pulse sequences to the assignment of ^{13}C spectra in labelled biomolecules.

7.1.1 Scalar Correlation

Through-bond correlation spectroscopy mediated by J–couplings is well established in solution–state NMR [43]. The main ingredient of though-bond correlation spectroscopy in solid–state NMR is to construct a mixing pulse sequence that allows only J–couplings to be active while suppressing all other interactions. In terms of the symmetry notation such a sequence should allow only $\{m, \mu\} = \{0, 0\}$ components, while suppressing all CSA and through-space dipole-dipole coupling terms. One suitable symmetry is $C9_3^1$ [44]. Many others are known [4].

A schematic of a scalar correlation experiment using a $C9_3^1$ sequence as a mixing element is shown in Fig. 8a. An experimental spectrum of [U–^{13}C,^{15}N]–bacteriochlorophyll is shown in Fig. 8b [45]. The cross–peaks reveal ^{13}C resonances belonging to sites with a mutual J–coupling. Similar results have been obtained on an U–^{13}C labelled cyclic decapeptide antamanide yielding assignments of most ^{13}C peaks [45].

In this context, we would like to point out that the RFDR pulse sequence [26–28], which is often proposed to be a dipole-dipole mixing sequence, in fact often generates an average Hamiltonian with a substantial J-coupling component [**?**]. Many RFDR spectra which have been interpreted in terms

of pure dipole-dipole couplings may be better understood as through-bond correlation spectra.

7.1.2 Double–Quantum Correlation

The INADEQUATE experiment [49] is widely employed in solution–state NMR for assigning ^{13}C spectra. Double–quantum correlation spectroscopy has similar potential in solid–state NMR by allowing only signals passing through DQ coherences and suppressing signals from isolated spins–$\frac{1}{2}$. This is particularly useful in large ^{13}C labelled biomolecules where the background signals from naturally–occuring isolated ^{13}C nuclei obscure the spectrum. As shown earlier $C7_2^1$ is a suitable candidate for DQ correlation spectroscopy [33]. This symmetry–based sequence recouples homonuclear DQ couplings. A similar sequence more suitable for high MAS frequencies is $C14_4^5$ [35]. This sequence can be made more efficient by adding supercycles to reduce resonance offset effects and CSA effects. This sequence is called SC14 and it recouples DQ dipole–dipole terms with the quantum numbers $\{l, m, \lambda, \mu\} = \{2, \pm 1, 2, \mp 2\}$ [35].

A typical pulse scheme employing SC14 for DQ correlation spectroscopy is shown in Fig. 9a. A 2D DQ spectrum of [U–^{13}C]-L–tyrosine is shown in Fig. 9b. All the assignments are clearly visible and marked in the spectrum.

DQ filtration effectively eliminates the natural abundance background from large biomolecules. Fig. 10 shows the ^{13}C spectrum of [11,12-$^{13}C_2$-retinylidene] bovine rhodopsin, compared with the corresponding double quantum filtered signal obtained using a $R14_2^6$ sequence [53]. DQ dipolar recoupling is a key step in many experiments for the determination of structural information, including internuclear distance and torsion angle measurements (see below).

Many other symmetries suitable for homonuclear DQ recoupling are available [4].

7.1.3 Homonuclear Zero–Quantum Recoupling

Homonuclear dipolar recoupling methods allow determination of proximity, distance and angular information under high–resolution MAS conditions. Besides the 2Q correlation spectroscopy discussed above, zero–quantum homonuclear dipolar recoupling may be used for obtaining 2D longitudinal magnetisation exchange spectra which yield a qualitative estimate of spatial proximity of spin sites, and which can identify resonances originating in the same spin system, even if the associated spins do not have a direct mutual coupling [50, 51]. A good ZQ sequence should be practically feasible at high MAS frequencies, should have minimum dependence on isotropic and anisotropic chemical shifts, have a low rf field requirement, and the recoupled DD interaction should be as large as possible.

A good candidate for ZQ homonuclear dipolar recoupling is the symmetry sequence $R6_6^2$. This recouples the DD terms with the following quantum numbers $\{l, m, \lambda, \mu\} = \{2, \pm 1, 2, 0\}$ and $\{2, \pm 2, 2, 0\}$ [52]. A pulse sequence for ZQ homonuclear dipolar recoupling is shown in Fig. 11a. An experimental 2D correlation spectrum of [U–^{13}C]-L–tyrosine acquired with the sequence in Fig. 11a is shown in Fig. 11b. The large number of cross–peaks in this spectrum show that the longitudinal magnetisation has been redistributed over the whole spin system by the zero–quantum recoupling sequence. This is the solid–state analogue of the TOCSY experiment in liquids. Ref. [4] lists many other symmetries suitable for homonuclear zero-quantum recoupling.

7.2 Local Geometry Determination

7.2.1 Heteronuclear Distance Measurements and H-Bond Effects

Heteronuclear distance measurements are very useful for molecular structure refinements and for investigating protein secondary structure and hydrogen bondings. Separated local field (SLF) spectroscopy is a classic method for determining heteronuclear dipolar couplings and hence ^{13}C–^{1}H and ^{15}N–^{1}H

bond lengths [54,55]. In this 2D technique the chemical shifts in one dimension are correlated with the heteronuclear dipolar couplings in the other dimension. This high–resolution method normally uses simple multiple–pulse sequences for decoupling the homonuclear dipolar interactions. Although originally developed for static samples, it may also be used under MAS [**?**]. However, the MAS frequency must be slow enough to ensure sufficient sideband intensity from which both the magnitude and the orientation of the dipolar tensors may be estimated. In multiply-labelled samples, a high MAS frequency is required to ensure a good resolution and sensitivity. TC5 [56], TMREV [57,58] and R-sequences [4,59] have been used at high spinning frequencies, although only the R-sequences have theoretically ideal behaviour in the first-order theory.

Figure 12a shows a SLF pulse scheme involving a RN_n^ν sequence for heteronuclear dipolar recoupling. Fig. 12b shows a ^{13}C 2D spectra obtained on [U-^{13}C]-L-histidine·HCl·H_2O at 10.9 kHz spinning frequency [59]. The splittings in the indirect dimension are proportional to heteronuclear DD couplings. Distance estimates are obtained by comparing the dipolar patterns with numerically exact two–spin simulations [36]. Table 2 summarizes the CH bond lengths of L-histidine·HCl·H_2O determined by neutron diffraction [60] and by solid-state NMR. Notice that the NMR bond lengths are consistently longer than neutron diffraction data due to the librational motion of the C-H bond in a direction orthogonal to the bond [**?**].

In order to quantify CH or NH bond elongations due to the formation of H-bonds, an internal calibration can be used. Fig. 12d shows the ^{15}N 2D spectra using $R18_2^5$ at 20 kHz spinning speed on uniformly ^{15}N labelled L-histidine·HCl·H_2O. The δ_1 ^{15}N–^{1}H bond is found to be about 4 pm longer than ϵ_1 ^{15}N–^{1}H bond due to the formation of an intermolecular hydrogen bond [59].

7.2.2 Homonuclear Distances: Bond Length Determination

The accurate determination of distances between like nuclei is of great importance. For good quality crystals of small molecules, diffraction methods give very accurate internuclear distances. For large biomolecules, on the other hand, the typical resolution from diffraction is of the order of 10 pm to 30 pm, after refinement.

For typical ^{13}C–^{13}C bonds in conjugated chains, the single bond distance is about 150 pm while the double bond distance is about 135 pm. These correspond to rather different electronic distributions. While single bonds are typically very flexible, isolated double bonds are quite stiff and the electrons forming the double-bond are expected to be localised between the two nuclei. Many conjugated systems exhibit intermediate bond orders and the bonding electrons are much more delocalised. In such cases, high-precision bond length measurements allow one to answer questions about reaction mechanism, electronic distribution and molecular motions.

Solid–state NMR can often provide such information. Internuclear distance measurements can be performed for directly bonded carbon pairs, using RN_n^ν-sequences for homonuclear DQ dipolar recoupling [61]. The precision is not yet as good for longer distances, although a variety of methods is available [19, 62].

A pulse sequence for distance measurements between homonuclear spin pairs is given in Fig. 13a. The DQ-filtered signal intensity depends upon the duration of the recoupling sequence. This is demonstrated experimentally in Fig. 13b for the case of [11,12-$^{13}C_2$]-all-*E*-retinal, a model of which is shown alongside the spectrum. This series of spectra was acquired using a fixed reconversion time, τ_{rec}, while τ_{exc} is incremented. The dipole-dipole interaction between the labelled nuclei is recoupled and the observed signals are modulated with a frequency which can be related to the strength of the dipole-dipole coupling constant and, hence, to the internuclear distance. Fig. 13d shows a typical best fit of the experimental points, corresponding

to $r_{jk} = ... \pm ...$ pm [61]. The method is sufficiently precise to distinguish between pure single bonds and double bonds, as well as intermediate cases in conjugated chains [61].

7.2.3 Torsion angle measurements

The torsion angles of four-atom units is a very important structural parameter. In NMR, torsion angles can be estimated by determining the relative orientation of a pair of anisotropic spin interaction tensors, such as CSA and DD coupling tensors. Methods have been developed to correlate the orientations between two CSA tensors [65], two dipolar tensors [66] and one CSA tensor with a dipolar tensor [63, 64]. The choice of dipolar tensors is preferred because the dipolar tensor is symmetric and precisely aligned along the internuclear vector. The orientation of a CSA tensor, on the other hand, depends on the local molecular structure and needs to be determined in advance by other methods.

A variety of experiments has been suggested for the determination of torsion angles [63,64,67,68]. Here, we outline an approach using symmetry–based pulse sequences leading to a direct measurement of a molecular torsion angle through the relative orientation of two magnetic spin–spin coupling tensors. We outline a method demonstrating the measurement of H–C–C–H torsion angles in $^{13}C_2$–labelled H–C–C–H moieties. 2Q coherence between isotopically labelled neighbouring ^{13}C sites are excited (for instance, by a $C7_2^1$ sequence) and are allowed to evolve in the presence of local fields from the directly–bonded ^{1}H spins. The heteronuclear dipolar fields depend on the spin states of the protons and also on the geometric relationship of the two ^{13}C–^{1}H coupling tensors. The experiment monitors the effect of heteronuclear dipolar interactions which are time–modulated due to MAS on the 2Q ^{13}C coherences generating a modulation of the ^{13}C 2Q evolution that depends on the H–C–C–H torsion angle. This is the solid–state NMR equivalent of double–quantum cross-correlation NMR in liquids [**?**, **?**].

The pulse sequence for determining the H–C–C–H torsion angle is given in Fig. 14a [70]. The amplitude of the 2Q signal is measured for a sufficient number of 2Q t_1 intervals. This method has been applied to the measurement of torsion angles in [10,11–$^{13}C_2$]–rhodopsin [69]. Simulations indicate that a torsion angle resolution of $\approx \pm 20^{o}$ can be achieved in the neighbourhood of the *cis* conformation and $\approx \pm 10^{o}$ in the neighbourhood of the *trans* conformation. A clear distinction between *cis* and *trans* conformations is easily achieved [70].

8 Conclusions

In this review an outline of the design of pulse sequences in solid–state NMR based on the symmetry properties of the spin interactions was given. Two classes of symmetry-based sequences were highlighted, namely, CN_n^{ν} and RN_n^{ν} . Representative applications of these sequences in various small biomolecular systems were highlighted. It is expected that a systematic application of these sequences will pave the way for an understanding of various structural and functional aspects of many biological systems. Work along these lines is being done in our group and several other research groups.

9 Acknowledgements

We thank Andreas Brinkmann and Ole Johannessen for various discussions and EPSRC (UK) for funding.

References

[1] Duer, M. J. (Editor) 2002, Solid State NMR Speectroscopy, Prinicples and Applications, Blackwell Science, UK.

[2] Bennett, A. E., Griffin, R. G., Vega, S. (1994) NMR Basic Principles and Progress, 33, 1.

[3] Dusold, S., and Sebald, A. 2000, Ann. Rep. NMR Spectrosc., 41, 185.

[4] Levitt, M. H. 2002, Encyc. Nucl. Magn. Reson., 9, 165, Wiley, UK.

[5] Andrew, E. R., Bradbury, A., and Eades, R. G. 1959, Nature, 183, 1802.

[6] Lowe, I. J. 1959, Phys. Rev. Lett., 2, 285.

[7] Bennett, A. E., Rienstra, C. M., Auger, M., Lakshmi, K. V., and Griffin, R. G. 1998, J. Chem. Phys., 103, 6951.

[8] Detken, A, Hardy, E. H., Ernst, M., and Meier, B. H. 2002, Chem. Phys. Lett., 141, 78.

[9] Pines, A., Gibby, M. G., and Waugh, J. S. 1973, J. Chem. Phys. 59, 569.

[10] Levitt, M. H. 2001, Spin Dynamics. Basics of Nuclear Magnetic Resonance, Wiley, Chichester, UK.

[11] Hartmann, S. R., and Hahn, E. L. 1962, Phys. Rev., 128, 2042.

[12] Peersen, O. B., Wu, X. L., Kustanovich, I., and Smith, S. O. 1993, J. Magn. Reson. A104, 334.

[13] Stejskal, E. O., Schaefer, J., and Waugh, J. S. 1977, J. Magn. Reson., 28, 105.

[14] Mehring, M. 1983, Prinicples of High Resolution NMR in Solids, Springer–Verlag, Berlin.

[15] Emsley, L., Laws, D. D., and Pines, A. 1999, Proc. Int. Sch. Phys. "Enrico Fermi", 129, 45.

[16] Yarim–Agaev, Y., Tutunjian, P. N., and Waugh, J. S. 1982, J. Magn. Reson., 47, 51.

[17] Raleigh, D. P., Levitt, M. H., and Griffin, R. G. 1988, Chem. Phys. Lett., 146, 71.

[18] Gan, Z. –H., and Grant, D. M. 1989, Mol. Phys. 67, 1419.

[19] Levitt, M. H., Raleigh, D. P., Creuzet, F., and Griffin, R. G. 1990, J. Chem. Phys. 90, 6347.

[20] Oas, T. G., Griffin, R. G., and Levitt, M. H. 1988, J. Chem. Phys., 89, 692.

[21] Smith, S. O., Aschheim, K., and Groesbeek, M., 1996, Quarterly Rev. Biophys., 29, 395.

[22] Gullion, T., and Schaefer, J. 1989, J. Magn. Reson., 81, 196.

[23] Gullion, T., and Schaefer, J. 1989, Adv. Magn. Reson., 13, 57.

[24] Tycko, R., and Dabbagh, G. 1990, Chem. Phys. Lett., 173, 461.

[25] Tycko, R., and Dabbagh, G. 1991, J. Am. Chem. Soc., 113, 9444.

[26] Bennett, A. E., Ok, J. H., Griffin, R. G., and Vega, S. 1992, J. Chem. Phys., 96, 8624.

[27] Sodickson, D. K., Levitt, M. H., Vega, S., and Griffin, R. G. 1993, J. Chem. Phys., 98, 6742.

[28] Ishii, Y. 2001, J. Chem. Phys., 114, 8473.

[29] Nielsen, N. C., Bildsøe, H., Jakobsen, H. J., and Levitt, M. H. 1994, J. Chem. Phys., 101, 1805.

[30] Tycko, R., and Smith, S. O. 1993, J. Chem. Phys., 98, 932.

[31] Edén, M., and Levitt, M. H. 1999, J. Chem. Phys., 111, 1511.

[32] Brinkmann, M., and Levitt, M. H. 2001, J. Chem. Phys., 115, 357.

[33] Lee, Y. K., Kurur, N. D., Helmle, M., Johannessen, O. G., Nielsen, N. C., and Levitt, M. H. 1996, Chem. Phys. Lett., 242, 304.

[34] Carravetta, M, Edén, M., Zhao, X., Brinkmann, M., and Levitt, M. H. 2000, Chem. Phys. Lett., 321, 205.

[35] Brinkamnn, M., Edén, M., and Levitt, M. H. 2000, J. Chem. Phys., 112, 8539.

[36] Zhao, X, Edén, M., and Levitt, M. H. 2001, Chem. Phys. Lett., 342, 353.

[37] Tycko R. 2001, Annu. Rev. Phys. Chem. 52, 575.

[38] van Beek, J. D., Hess, S., Vollrath, F., Meier, and B. H. 2002, Proc. Natl. Acad. Sci., 2002, 99, 10266.

[39] Asakura, T., Yao, J. M., Yamane, T., Umemura, and K. Ultrich, A. S. 2002, J. Am. Chem. Soc., 124, 8794.

[40] Lindstrom, F., Bokvist, M., Sparrman, T., and Grobner, G. 2002, Phys. Chem. Chem. Phys., 4, 5524.

[41] Kimura, S., Naito, A., Tuzi, S., and Saito, H. 2002, J. Mol. Struct., 602, 125.

[42] Ladizhansky, V., Veshtort, M., and Griffin, R. G. 2002, J. Magn. Reson., 154, 317.

[43] Ernst, R. R., Bodenhausen G., and Wokaun, A. 1987, Principles of Nuclear Magnetic Resonance in One and Two Dimensions, Clarendon Press, Oxford.

[44] Heindrichs, A. S. D., Geen, H., Giordani, C., and Titman, J. T. 2001, Chem. Phys. Lett. 335, 89.

[45] Hardy, E. H., Verel, R, and Meier, B. H. 2001, J. Magn. Reson., 148, 459.

[46] Hediger, S., Meier, B. H., and Ernst, R. R. 1995, Chem. Phys. Lett., 240, 449

[47] Baldus, M., and Beier, B. H. 1996, J. Magn. Reson., A121, 65.

[48] Lee, M., and Goldburg, W. I. 1965, Phys. Rev. A, 140, 1261.

[49] Bax, A., Freeman, R., and Frenkiel, T. A. 1981, J. Am. Chem. Soc., 103, 2102.

[50] Boender, G. J., Raap, J., Prytualla, S., Oschkinat, H., and de Groot, H. J. M. 1995, Chem. Phys. Lett., 237, 502.

[51] McDermott, A., Polenova, T., Bockmann, A., Zilm, K. W., Paulsen, E. K., Martin, R. W., and Montelione, G. T. 2000, J. Biomol. NMR., 16, 209.

[52] Brinkmann, A., Schmedt auf der Günne, J., and Levitt, M. H. 2002, J. Magn. Reson., 156, 79.

[53] Carravetta, M. unpublished results.

[54] DiVerdi, J. A., Opella, S. 1982, J. Am. Chem. Soc., 104, 1761.

[55] Roberts, J. E., Harbison, G. S., Munowitz, M. G., Herzfeld, J., Griffin, R. G. (1987) J. Am. Chem. Soc., 109, 4163.

[56] Gross, J. D., Costa, P. R., Griffin, R. G. (1998) J. Chem. Phys. 108, 7286.

[57] Howhy, M., Jaroniec, C. P., Reif, B., Rienstra, C. M., Griffin, R. G. (2000) J. Am. Chem. Soc., 122, 3218.

[58] Reif, B., Hohwy, M., Jaroniec, C. P., Rienstra, C. M.m Griffin, R. G. (2000) J. Magn. Reson., 145, 132.

[59] Zhao, X., Sudmeier, J. L., Bachovchin, W. W., Levitt, M. H. (2001) J. Am. Chem Soc. 123, 11097.

[60] Fuess, H., Hohlwien, D., Mason, S. A. 1977, Acta Cryst., B33, 654.

[61] Carravetta, M., Edén, M., Johannessen, O. G., Luthman, H., Verdegem, P. J. E., Lugtenburg, J., Sebald, A., Levitt, M. H. (2001) J. Am. Chem. Soc., 123, 10628.

[62] Gregory, D. M., Mitchell, D. J., Stringer, J. A., Kiihne, S., Shiels, J. C., Callahan, J., Mehta, M. A., Drobny, G. P. 1995, Chem. Phys. Lett., 246, 654.

[63] Weliky, D. P., Dabbagh, G., Tycko, R. 1993, J. Magn. Reson. A104, 10.

[64] Dabbagh, G., Weliky, D. P., Tycko, R. 1994, Macromolecules, 27, 6183.

[65] Weliky, Tycko, R. 1996, J. Am. Chem. Soc. 118, 8487.

[66] Fujiwara, T., Shimomura, T., Ohigashi, Y., Akutsu, H. 1998, J. Chem. Phys., 109, 2380.

[67] Schmidt–Rohr, K. 1996, Macromolecules, 29, 3975.

[68] Schmidt–Rohr, K. 1996, J. Am. Chem. Soc., 118, 7601.

[69] Feng, X., Verdegem, P. J. E., Lee, Y. K., Sandström, D., Edén, M., Bovee–Geurts, P., de Grip, W. J., Lugtenburg, J., de Groot, H. J. M., Levitt, M. H. 1997, J. Am. Chem. Soc. 119, 6853.

[70] Feng, X., Lee, Y. K., Sandström, D., Edén, M., Maisel, H., Sebald, A., Levitt, M. H. 1996, Chem. Phys. Lett., 257, 314.

[71] Haeberlen, U. 1976, High resolution NMR in solids:Selective averaging, Supplement No. 1 to Adv. Magn. Reson. Academic Press, New York.

[72] Feng, X., Verdegem, P. J. E., Edén, M., Sandström, D., Lee, Y. K., Bovee–Geurts, P. H. M., de Grip, W. J., Lugtenburg, J., de Groot, H. J. M., and Levitt, M. H., 2000, J. Biomol. NMR., 16, 1.

Table 1: Rotational ranks of spin interactions in a diamagnetic solid.

Spin interaction	Space rank, l	Spin rank, λ
Isotropic chemical shift	0	1
Chemical shift anisotropy	2	1
J–coupling	0	0
Homonuclear Dipole–dipole coupling	2	2
Heteronuclear Dipole–dipole coupling	2	1^*

* rank under rotation of only one spin species

Table 2. Estimated ^{13}C–^{1}H and ^{15}N–^{1}H bond lengths in L–histidine.HCl.H_2O (pm)

Atom	Site	Neutron diffraction	Solid–state NMR
^{13}C	α	110.3	112.0
	β	109.7	111.0
	ϵ_1	108.9	109.0
	δ_2	107.6	108.5
^{15}N	ϵ_2	102.6	105.0
	δ_1	107.0	109.0

Figure Captions

Figure 1: (a) A schematic of the MAS technique showing the sample spinning at an angular frequency ω_r about an axis at the magic–angle of $\tan^{-1}\sqrt{2} \approx 54.7^{o}$ with respect to the static magnetic field, B_0. (b) A schematic of continuous–wave (CW) decoupling showing the pulse sequence for observation of rare spins such as ^{13}C while the heteronuclear interactions are suppressed by continuous–wave rf irradiation at the Larmor frequency of ^{1}H. (c) A schematic of the CP pulse sequence in which magnetisation transfer from ^{1}H to ^{13}C takes place by matching the rf fields on the ^{1}H and ^{13}C channels according to the Hartmann–Hahn condition. A decoupling field is applied to the ^{1}H channel while observing ^{13}C.

Figure 2: ^{13}C CP-MAS spectra of [$^{13}C_2$,^{15}N]–glycine at different spinning frequencies in a field of 9.4 T. The vertical scales of the spectra are: (a):(b):(c):(d):(e)=6:4:1:1:1. The MAS frequencies, $\omega_r/2\pi$ are indicated alongside each spectrum.

Figure 3: Schematic of a recoupling sequence showing the time–dependence of the heteronuclear dipolar coupling Hamiltonian, $\mathcal{H}_{IS}$ in the interaction frame of the rf field. (a) The time–dependent evolution of $\mathcal{H}_{IS}$ under MAS. The integral of the dipolar coupling over a single rotor cycle is zero leading to an averaging of the dipolar coupling to zero if the spinning speed is sufficiently high. On the right is shown an internuclear vector between a carbon nucleus and a nitrogen nucleus traversing a conical path. (b) The time–dependent evolution of $\mathcal{H}_{IS}$ under MAS with two π pulses on the S spin per rotor cycle. Since each π pulse reverses the sign of $\mathcal{H}_{IS}$ the dipolar coupling is no longer averaged to zero but gets scaled by κ, the scaling factor, depending on the nature of the pulse sequence applied for recoupling. (Reproduced with permission from Ref. [15]).

Figure 4: Construction of a CN_n^ν sequence. The pulse sequence is set up so that n sample revolutions are synchronised with N rf cycles. In the simplest version, the rf cycle may be a 2π pulse. The pulses of consecutive cycles increment in steps of $2\pi\nu/N$.

Figure 5: Spin–space selection (SSS) diagram for the symmetry $C7_2^1$ showing the selection of double–quantum dipolar and isotropic chemical shift terms, and symmetry–forbidden CSA terms. The space part, m, and the spin part, μ, are split for visual clarity. Only those branches with $m \geq 0$ are shown: the branches with $m < 0$ are mirror images. The $m = 0$ component vanishes in the case of exact MAS. For the symmetry $C7_2^1$, the space branches are spaced vertically by two units corresponding to $n = 2$. Each of these branches splits into three spin components, with $\mu = \{-1, 0, 1\}$, and are spaced vertically by one unit corresponding to $\nu = 1$. The barrier on the right has holes at levels 0, ± 7, ± 14, $\cdots$ corresponding to $N = 7$. A spin interaction component is symmetry–allowed if the corresponding branch passes through a hole in the barrier. If it does not pass through a hole, it symmetry–forbidden and is suppressed by the recoupling sequence, to first order.

Figure 6: Construction of a RN_n^ν sequence. The pulse sequence timing is set up so that n sample revolutions are synchronised with N rf elements. Each pulse element may be a simple π pulse or a composite π pulse. The phases of the elements alternate between the values $\pm\pi\nu/N$.

Figure 7: SSS diagram for the symmetry $R18_2^5$ showing (a) symmetry–allowed CSA/hetero-DD terms (b) symmetry–forbidden Homo–DD terms (c) symmetry–forbidden isotropic chemical shift terms. The position of the holes in the barrier depends on whether the spin rank λ is odd or even. In cases (a) and (c), the rank $\lambda = 1$ is odd, so the holes in the barrier are at levels $\pm 9, \pm 27 \ldots$. In case (b), the rank $\lambda = 2$ is even, so the holes in the barrier are at levels $0, \pm 18, \pm 36 \cdots$.

Figure 8: (a) Pulse sequence for 2D correlation spectroscopy employing the mixing sequence $C9_3^1$. The preparation period consists of a CP block generating ^{13}C magnetisation from ^{1}H. During the mixing period magnetisation transfer takes place under an isotropic mixing Hamiltonian generated by the $C9_3^1$ sequence bracketed by two $\frac{\pi}{2}$ pulses. (b) Part of a scalar correlation spectrum of [U–^{13}C, ^{15}N]-bacteriochlorophyll recorded using the pulse sequence in (a). See Ref. [44] for experimental details. (Reproduced with permission from Ref. [44]).

Figure 9: (a) Pulse sequence for 2Q correlation spectroscopy using the symmetry sequence, $C14_4^{-5}$ for 2Q excitation and conversion. I refers to ^{1}H and S refers to ^{13}C. Following ramped CP a $\pi/2$ pulse on S converts the transverse magnetisation into S spin longitudinal magnetisation. The $\pi/2$ pulse is followed by a 2Q–excitation pulse sequence of duration τ_E which converts the S–spin longitudinal magnetisation into (± 2)–quantum coherence. The 2Q coherences are allowed to evolve for a time interval of t_1, and are then reconverted into longitudinal S–spin magnetisation by another $C14_4^{-5}$ block. The longitudinal magnetisation is converted into observable magnetisation by a $\pi/2$ read pulse. (b) Experimental 2D 2Q ^{13}C spectrum of [U–^{13}C]–L–tyrosine. See Ref. [35] for experimental details. (Reproduced with permission from Ref. [35]).

Figure 10: (a) RAMP–CP ^{13}C spectrum of [11,12-$^{13}C_2$-retinylidene]-rhodopsin, acquired at 9.4 T and 173 K, at a spinning frequency of 5.5 kHz (b) Experimental 2D filtered spectrum acquired under the same conditions using the sequence $R14_2^6$ [53, 61]).

Figure 11: (a) Pulse sequence for zero–quantum correlation spectroscopy using the sequence $R6_6^2$ for the transfer of longitudinal magnetisation between neighbouring sites. (b) Experimental 2D homonuclear ^{13}C correlation spectrum of [U–^{13}C]–L–tyrosine at a spinning frequency of 23.0 kHz, and a mixing interval of 9.9 ms. (b) Experimental 2D 2Q ^{13}C spectrum of [U–^{13}C]–L–tyrosine. See Ref. [52] for experimental details. (Reproduced with permission from Ref. [52]).

Figure 12: (a) Pulse sequence for heteronuclear dipolar recoupling where the R sequence may be either $R18_1^7$ or $R18_2^5$. (b) Experimental ^{13}C 2D spectrum of [U-$^{13}C_6$,$^{15}N_3$]-L-histidine·HCl·H_2O at 9.4 T and a spinning frequency of 10.9 kHz with $R18_1^7$ sequence. (c) Sections through the 2D spectrum parallel to the ω_1 axis. These show the heteronuclear dipolar split patterns for each of the ^{13}C sites bonded with ^{1}H. (d) Experimental ^{15}N 2D spectrum of [U-$^{13}C_6$,$^{15}N_3$]-L-histidine·HCl·H_2O at 9.4 T and a spinning frequency of 20.0 kHz using $R18_2^5$. (e) Sections through the 2D spectrum parallel to the ω_1 axis. These show the heteronuclear dipolar split patterns for each of the ^{13}C sites bonded with ^{1}H. (Reproduced with permission from Ref. [36, 59])

Figure 13: (a) Pulse sequence used for the measurement of distances between homonuclear spin pairs. The sequence starts with RAMP–CP followed by a $\pi/2$ pulse, to create enhanced longitudinal magnetisation on the spin species S, in this case ^{13}C. This is followed by a recoupling interval of duration τ_{exc} to generate DQ coherences between the labelled spins. This is followed by an interval of duration τ_{rec} during which the DQ coherence is reconverted back to longitudinal magnetisation and then observed through a $\pi/2$ reading pulse. The whole reconversion block is phase cycled to select DQ coherences while suppressing all other terms at the end of the excitation block. (b) A series of double–quantum filtered spectra of [11,12-$^{13}C_2$]-all-*E*-retinal for different values of τ_{exc}. The molecular schematic is also shown. (c) Best fit of the experimental points indicating a distance of 137.6 ± 1.7 pm (Reproduced with permission from Ref. [61]).

Figure 14: (a) Pulse sequence for the measurement of H–C–C–H torsion angles using a $C7_2^1$ sequence for 2Q excitation and a MREV–8 [71] for homonuclear decoupling. (b) Coherence pathway diadram. (c) Signal amplitudes for [10,11–$^{13}C_2$]–metarhodopsin–I as a function of the 2Q evolution interval t_1. The filled circles correspond to experimental values. The lines correspond to best–fit simulations for H–C–C–H torsion angles of $|\phi| = 140^o, 160^o, 170^o$, and 180^o. The dotted lines indicated that the 68.3% confidence limits on the torsion angle are $\phi = 180 \pm 22^o$. (Reproduced with permission from Ref. [72]).

a

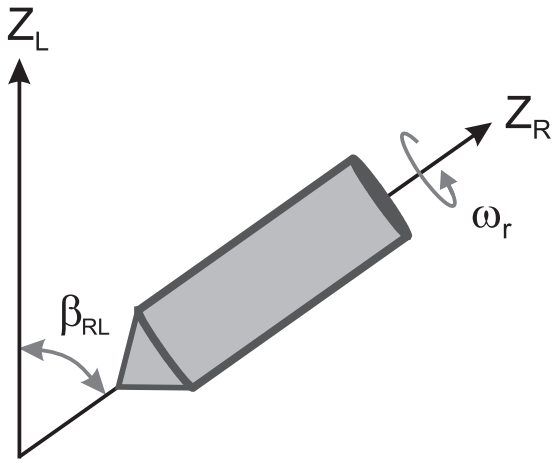
Z_L
Z_R
ω_r
β_{RL}

b

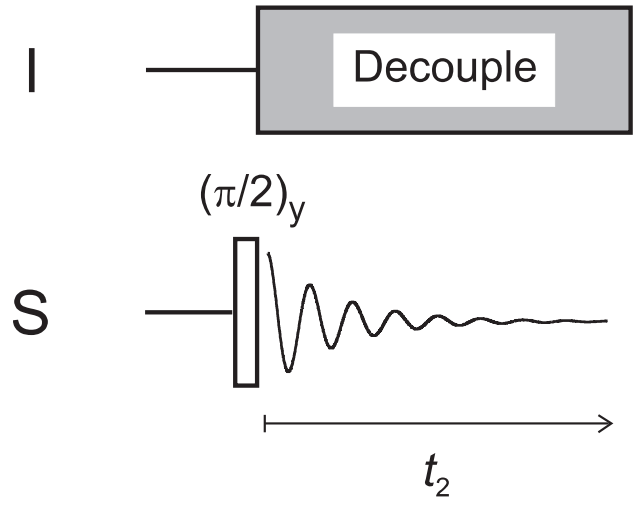
I
Decouple
$(\pi/2)_y$
S
t_2

c

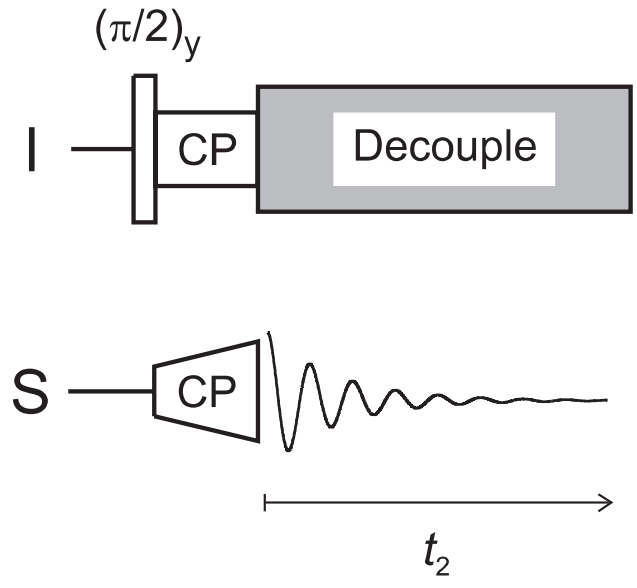
$(\pi/2)_y$
I
CP
Decouple
S
CP
t_2

Figure 1

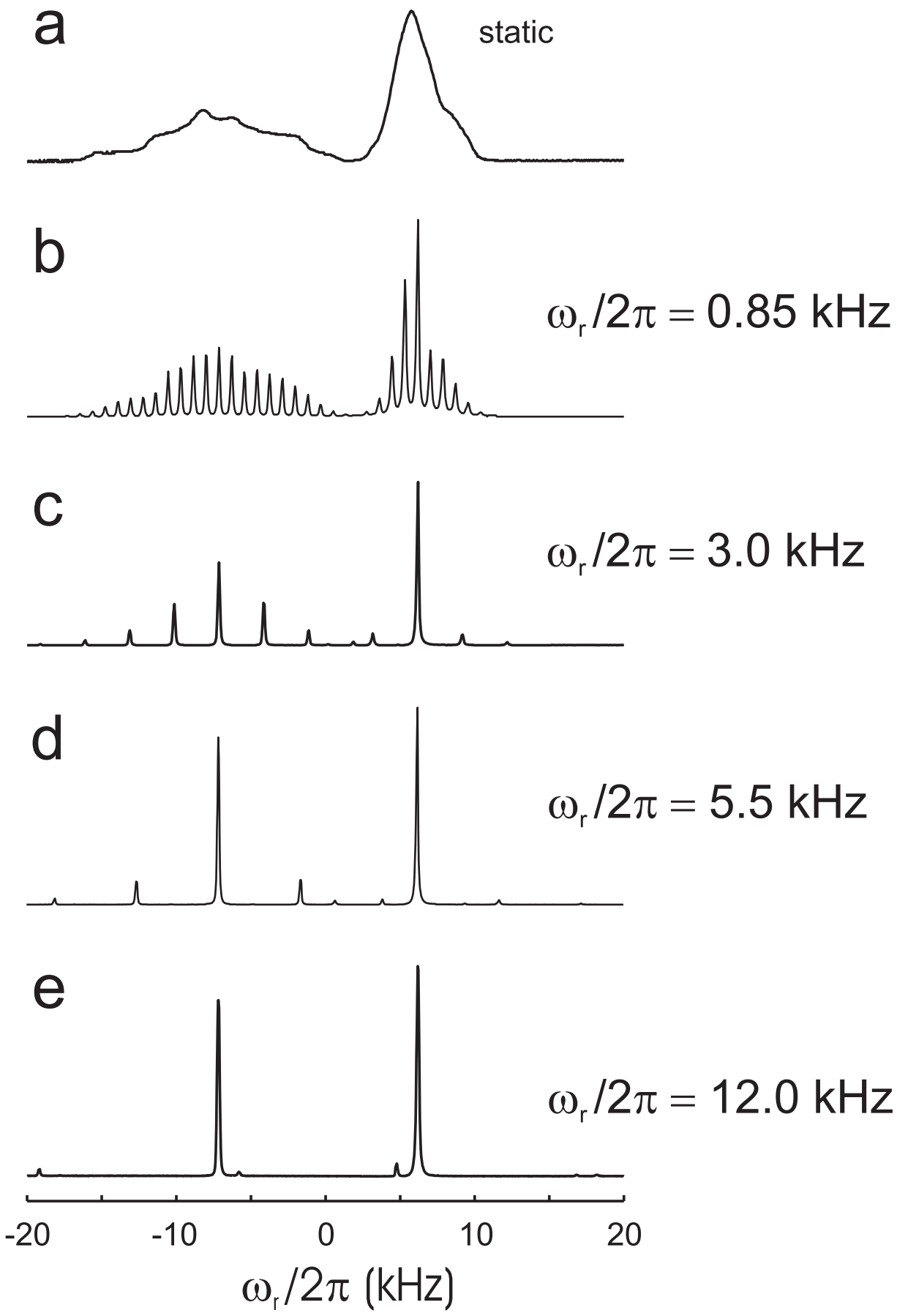
a
static
b
$\omega_r/2\pi = 0.85$ kHz
c
$\omega_r/2\pi = 3.0$ kHz
d
$\omega_r/2\pi = 5.5$ kHz
e
$\omega_r/2\pi = 12.0$ kHz
-20
-10
0
10
20
$\omega_r/2\pi$ (kHz)

Figure 2

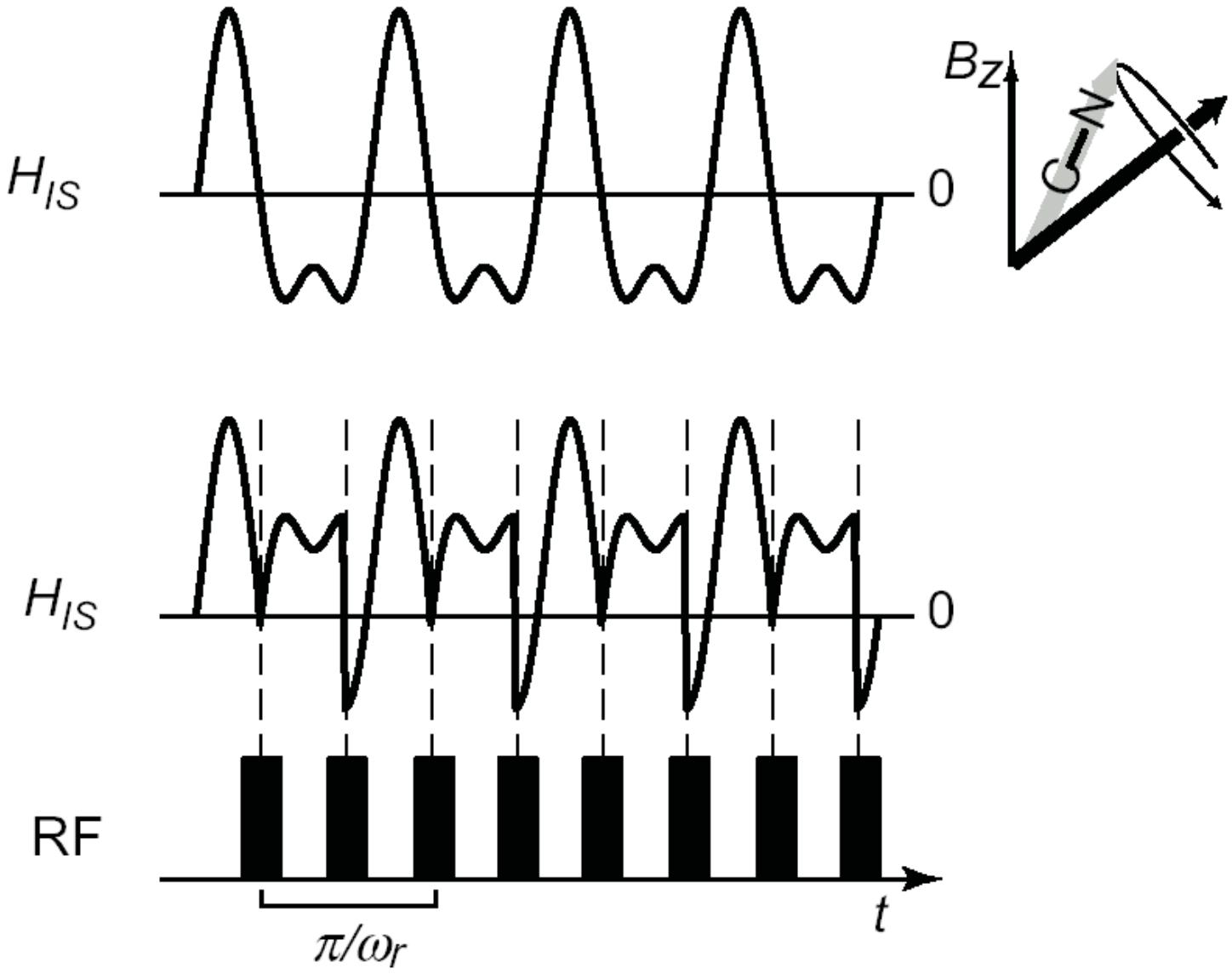

Figure 3

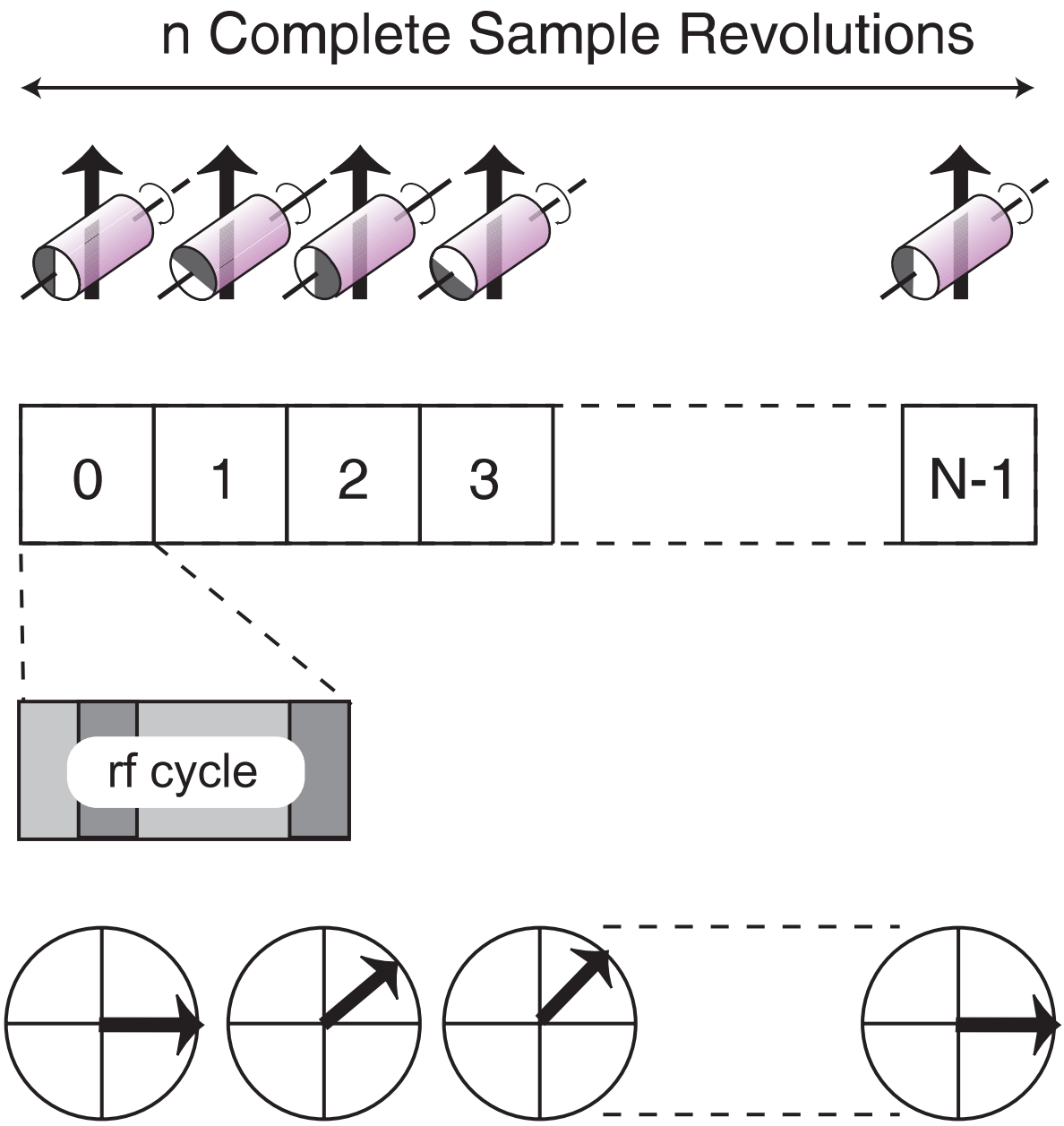
n Complete Sample Revolutions
0
1
2
3
N-1
rf cycle
rf phase incrementation +2πν/N

Figure 4

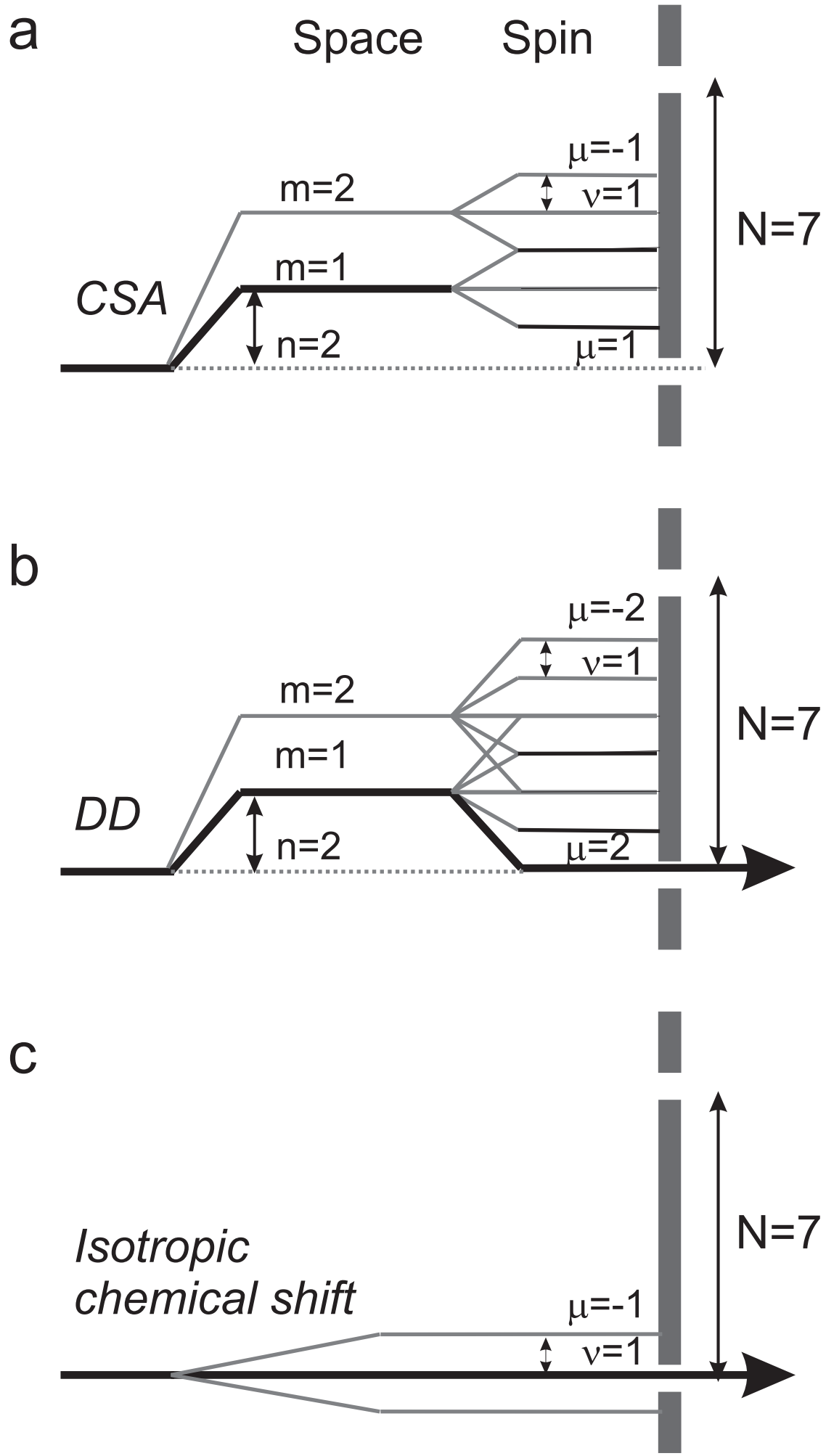
a
Space
Spin
μ=-1
ν=1
m=2
m=1
CSA
n=2
μ=1
N=7
b
μ=-2
ν=1
m=2
m=1
DD
n=2
μ=2
N=7
c
N=7
Isotropic
chemical shift
μ=-1
ν=1

Figure 5

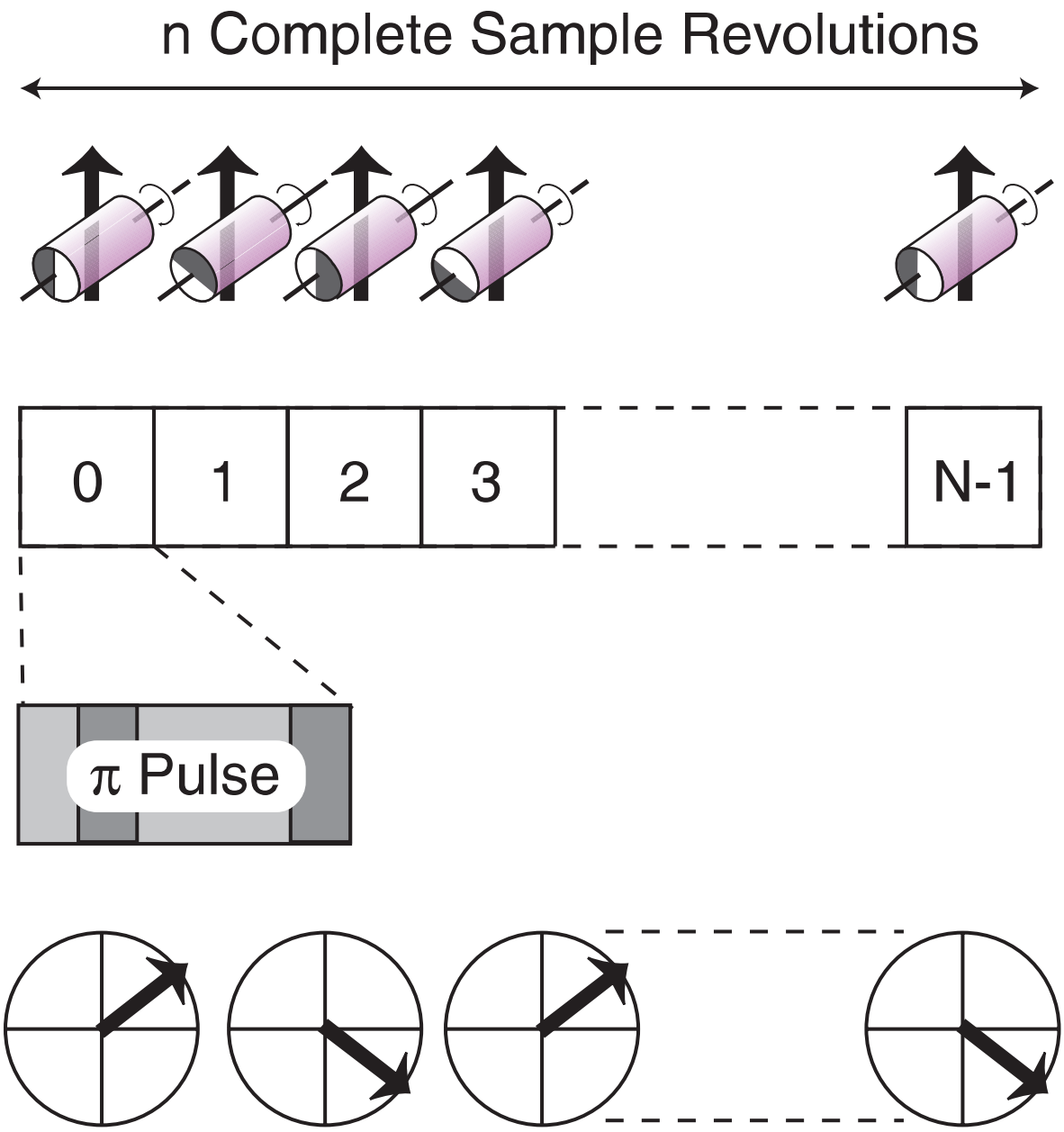
n Complete Sample Revolutions
0
1
2
3
N-1
π Pulse
rf phase incrementation ±πν/N

Figure 6

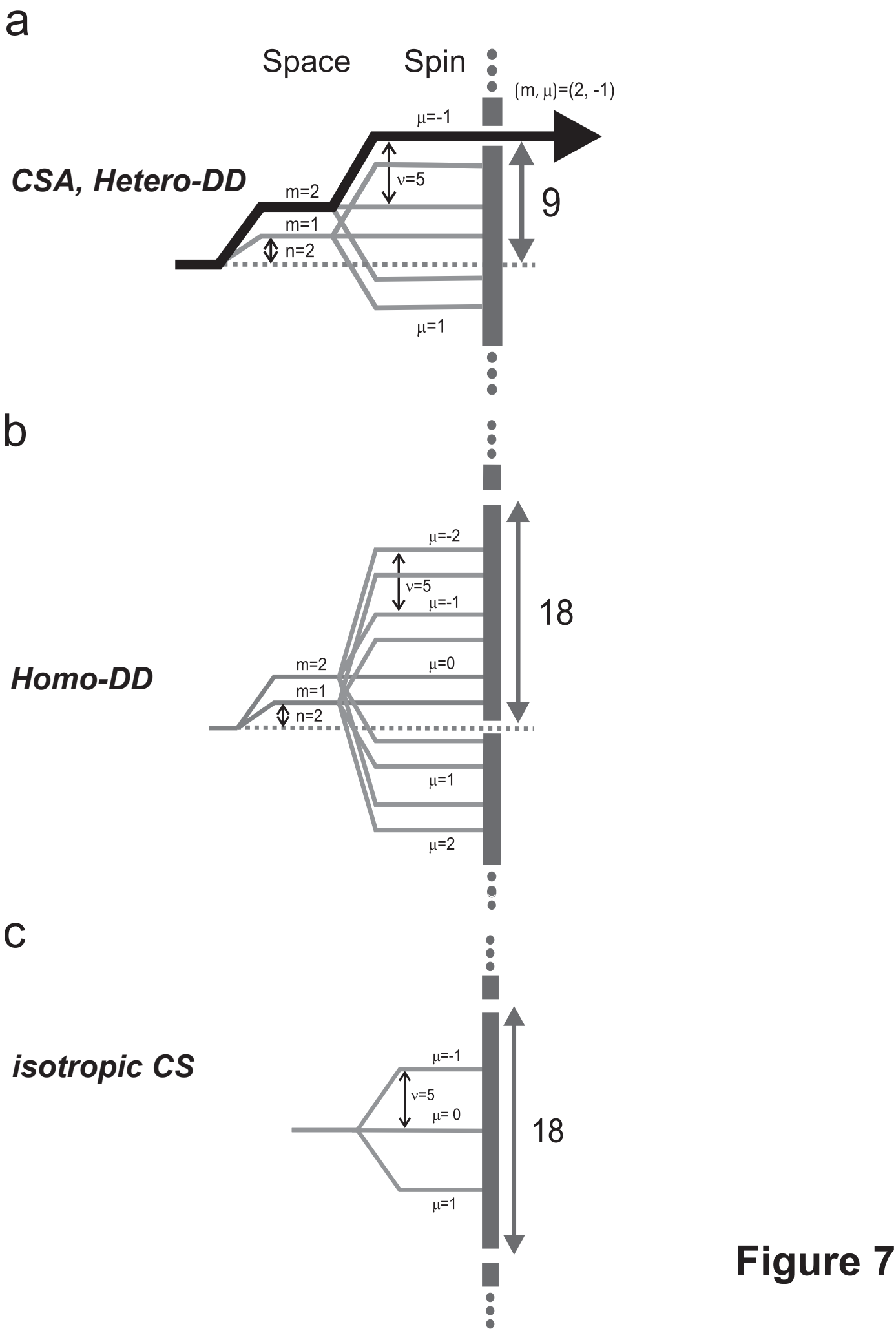
a
Space
Spin
(m, μ)=(2, -1)
μ=-1
CSA, Hetero-DD
ν=5
m=2
m=1
n=2
9
μ=1
b
μ=-2
ν=5
μ=-1
18
Homo-DD
m=2
μ=0
m=1
n=2
μ=1
μ=2
c
isotropic CS
μ=-1
ν=5
μ= 0
18
μ=1

Figure 7

a

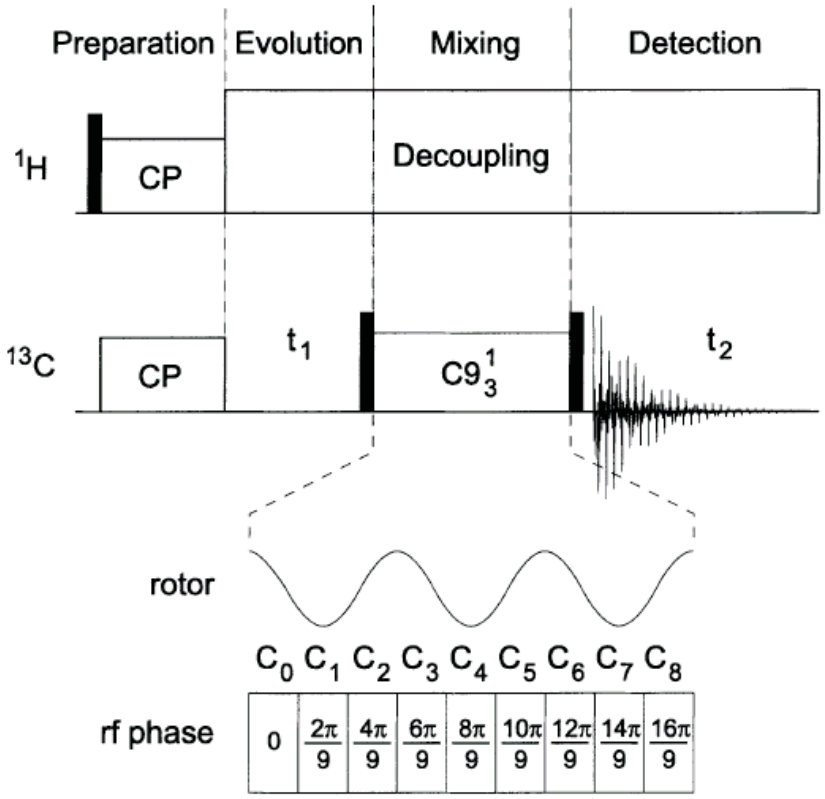
Preparation
Evolution
Mixing
Detection
^{1}H
CP
Decoupling
^{13}C
CP
t_1
$C9_3^1$
t_2
rotor
C_0 C_1 C_2 C_3 C_4 C_5 C_6 C_7 C_8
rf phase
0
$\frac{2\pi}{9}$
$\frac{4\pi}{9}$
$\frac{6\pi}{9}$
$\frac{8\pi}{9}$
$\frac{10\pi}{9}$
$\frac{12\pi}{9}$
$\frac{14\pi}{9}$
$\frac{16\pi}{9}$

b

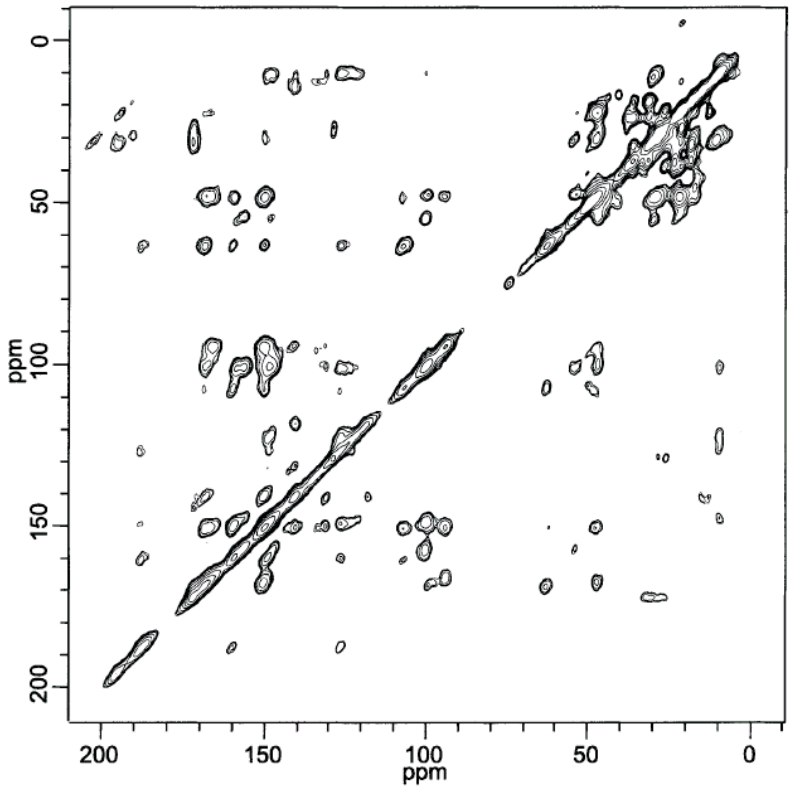
0
50
100
150
200
ppm
200
150
100
50
0
ppm

Figure 8

a

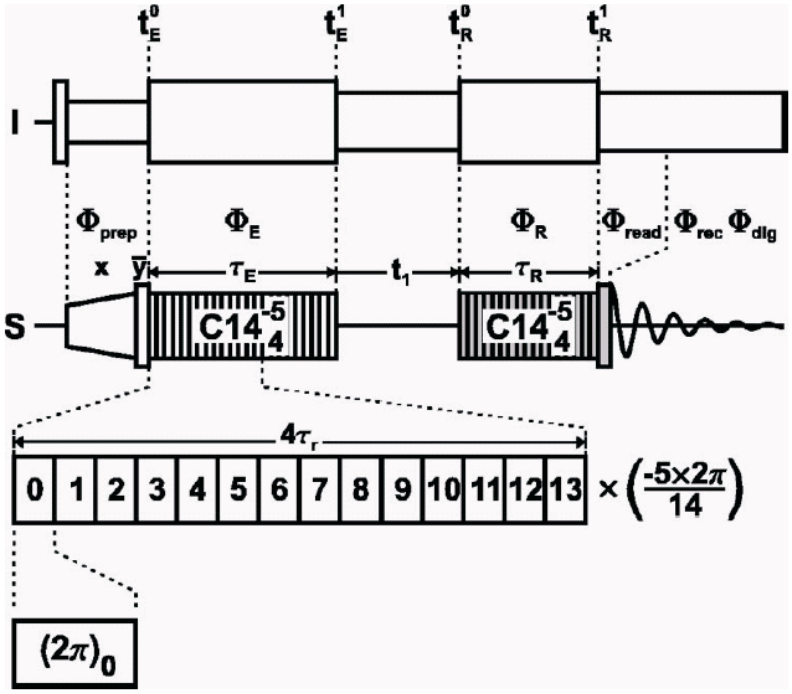
t_E^0
t_E^1
t_R^0
t_R^1
I
S
Φ_{prep}
Φ_E
Φ_R
Φ_{read}
Φ_{rec}
Φ_{dig}
x
$\bar{y}$
τ_E
t_1
τ_R
C14 -5 4
C14 -5 4
$4\tau_r$
0 1 2 3 4 5 6 7 8 9 10 11 12 13
$\times\left(\frac{-5\times 2\pi}{14}\right)$
$(2\pi)_0$

b

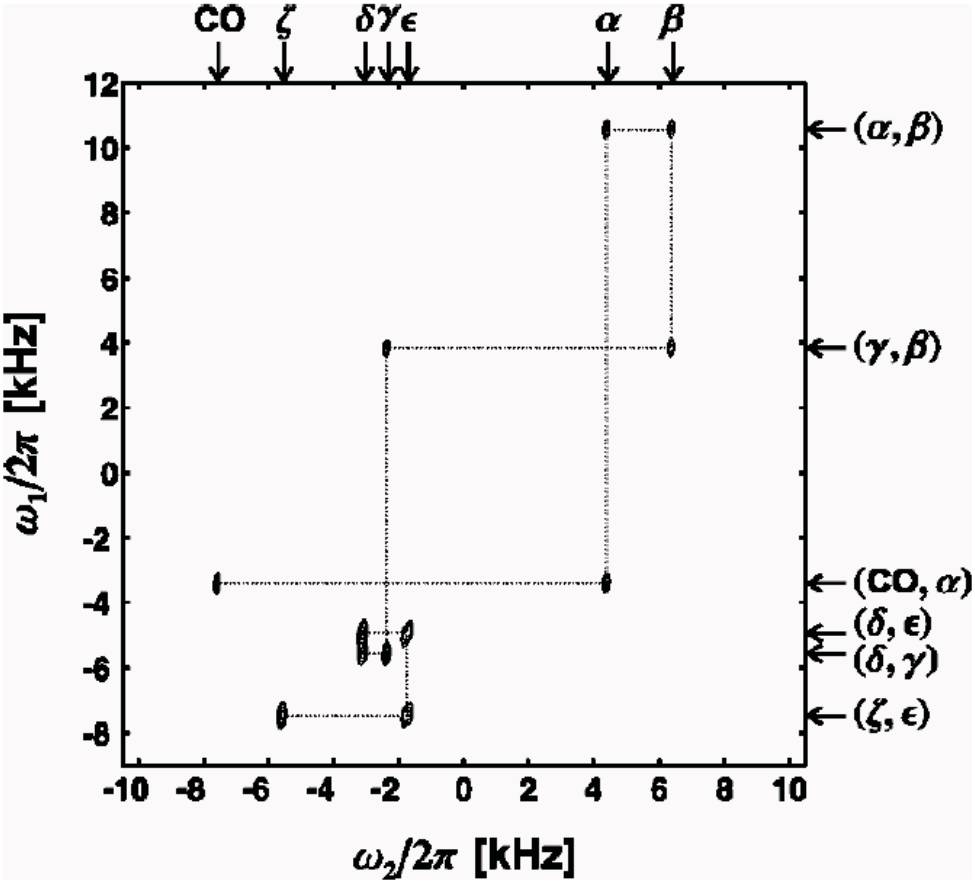
CO
ζ
δγϵ
α
β
12
10
8
6
4
2
0
-2
-4
-6
-8
-10 -8 -6 -4 -2 0 2 4 6 8 10
$\omega_1/2\pi$ [kHz]
$\omega_2/2\pi$ [kHz]
← (α, β)
← (γ, β)
← (CO, α)
← (δ, ϵ)
← (δ, γ)
← (ζ, ϵ)

Figure 9

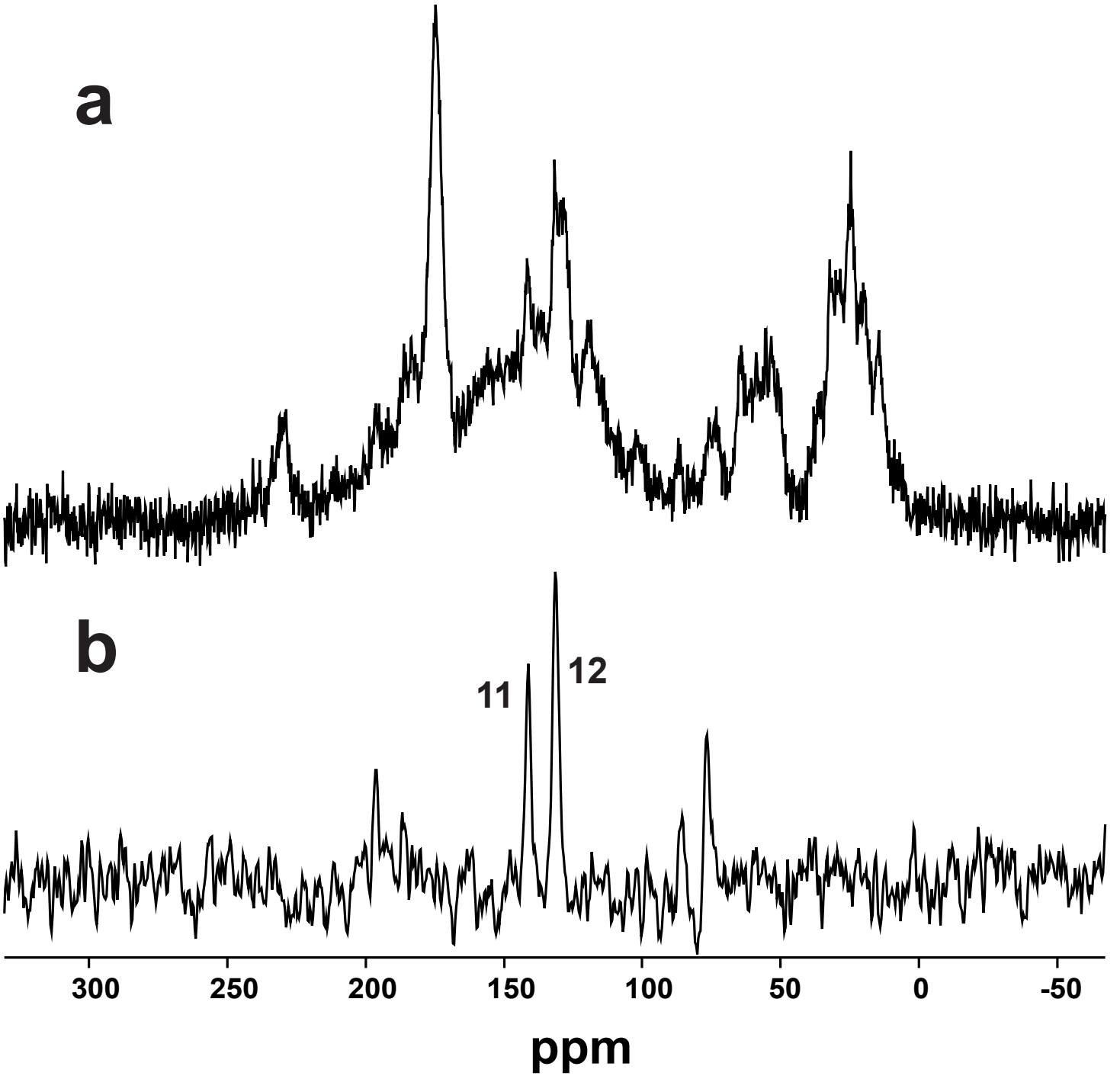

Figure10

a

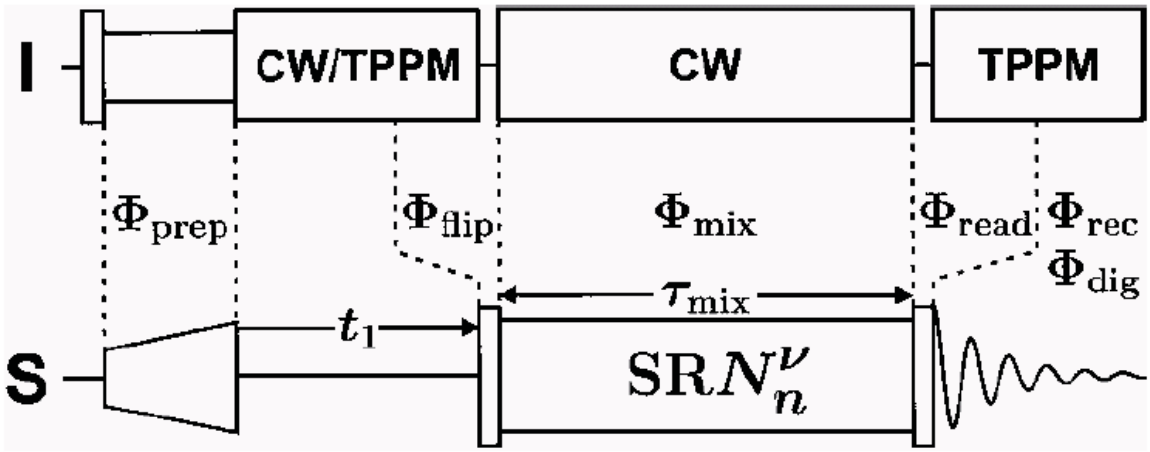
I
CW/TPPM
CW
TPPM
Φ_{prep}
Φ_{flip}
Φ_{mix}
Φ_{read}
Φ_{rec}
Φ_{dig}
τ_{mix}
t_1
S
SRN_n^ν

b

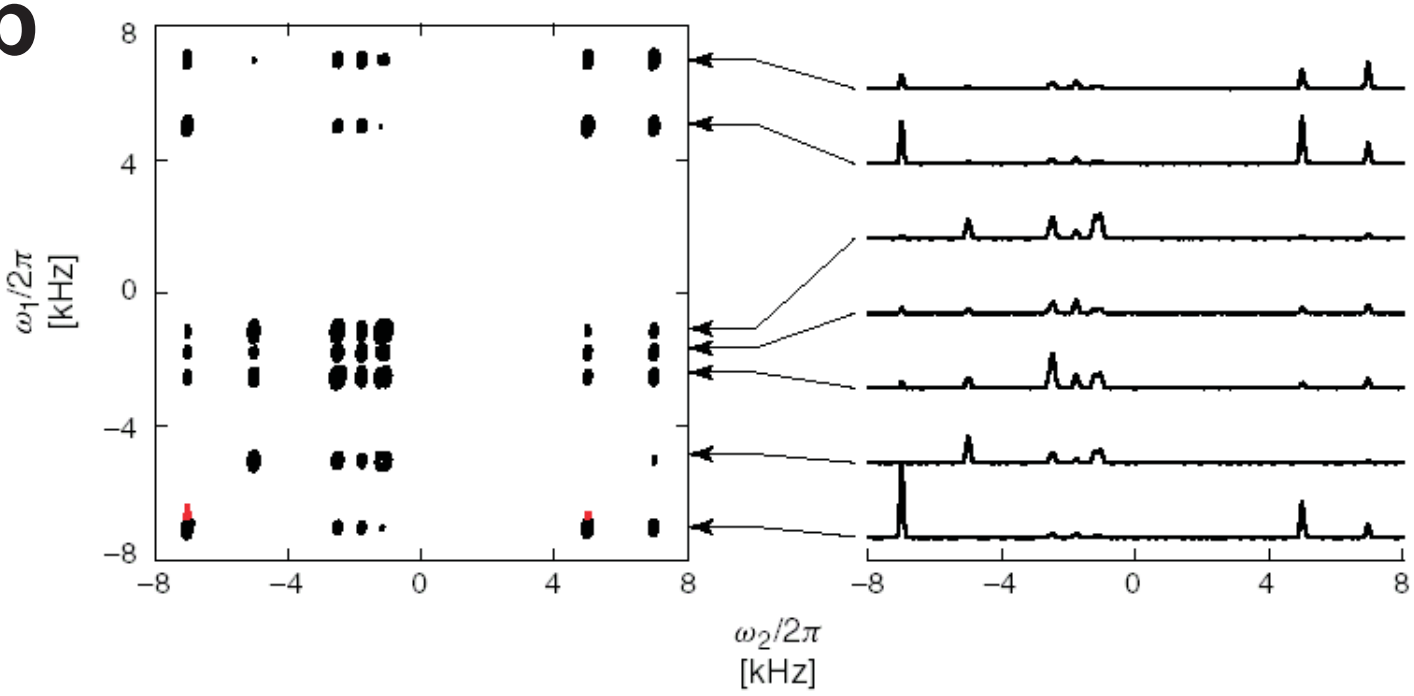
8
4
0
−4
−8
$\omega_1/2\pi$ [kHz]
−8
−4
0
4
8
$\omega_2/2\pi$ [kHz]

Figure 11

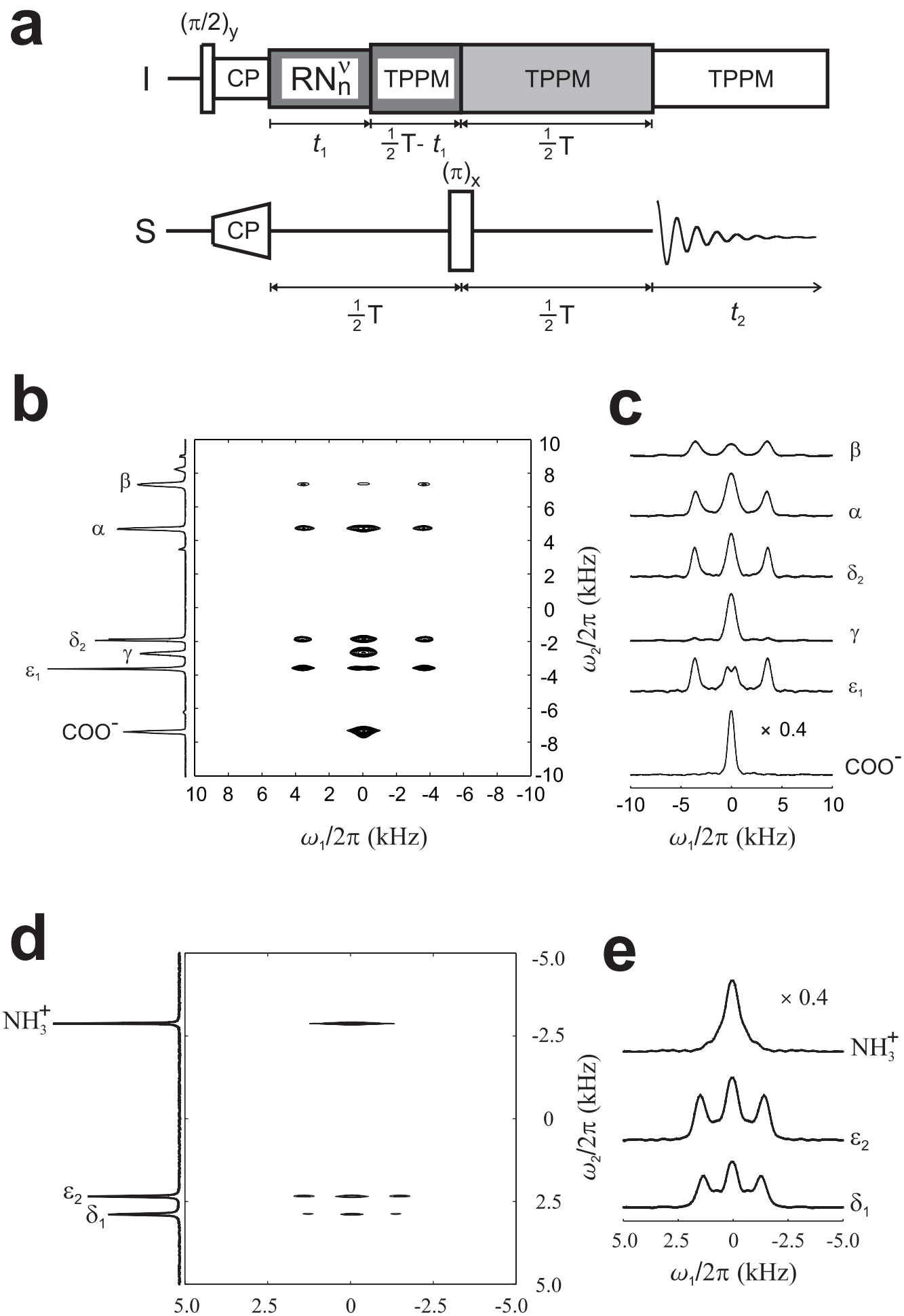
a
(π/2)y
I
CP
RNn^ν
TPPM
TPPM
TPPM
t1
½T- t1
½T
(π)x
S
CP
½T
½T
t2
b
β
α
δ2
γ
ε1
COO-
10 8 6 4 2 0 -2 -4 -6 -8 -10
ω1/2π (kHz)
ω2/2π (kHz)
c
β
α
δ2
γ
ε1
× 0.4
COO-
-10 -5 0 5 10
ω1/2π (kHz)
d
NH3+
ε2
δ1
5.0 2.5 0 -2.5 -5.0
ω1/2π (kHz)
ω2/2π (kHz)
e
× 0.4
NH3+
ε2
δ1
5.0 2.5 0 -2.5 -5.0
ω1/2π (kHz)

Figure 12

a

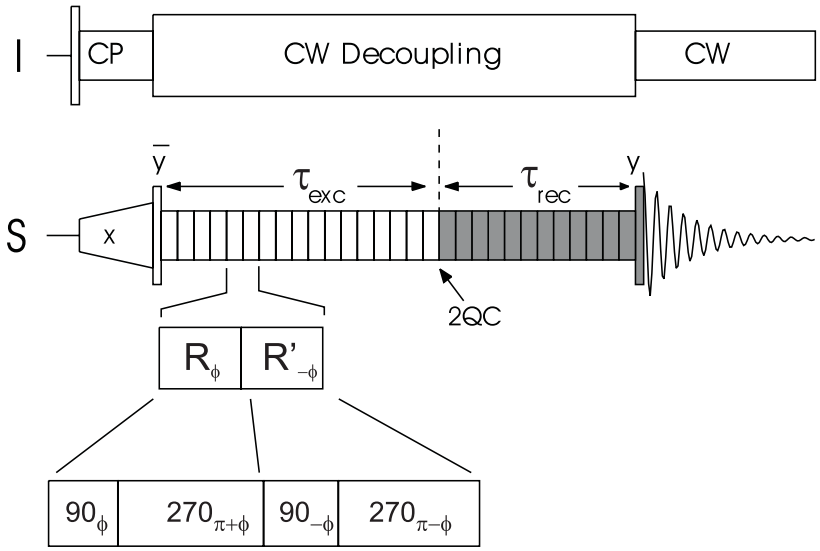

b

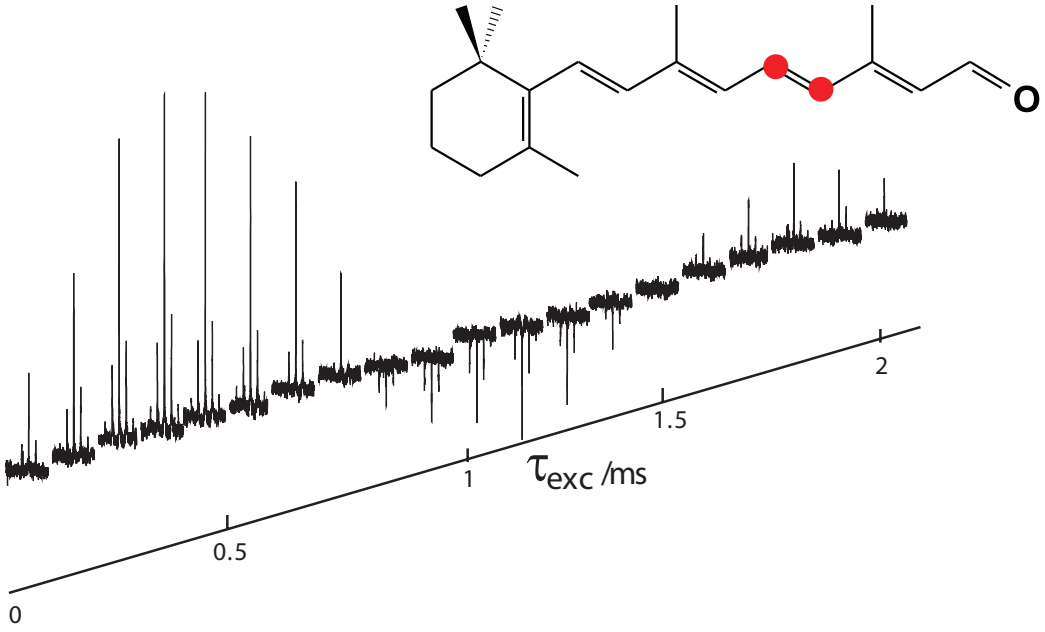

c

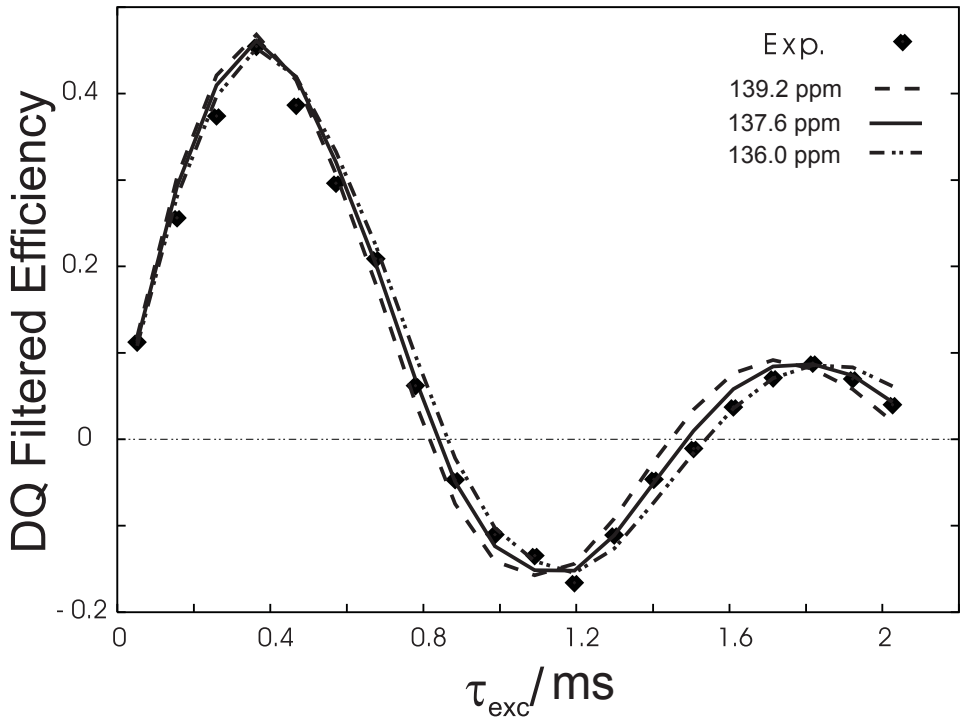

Figure 13

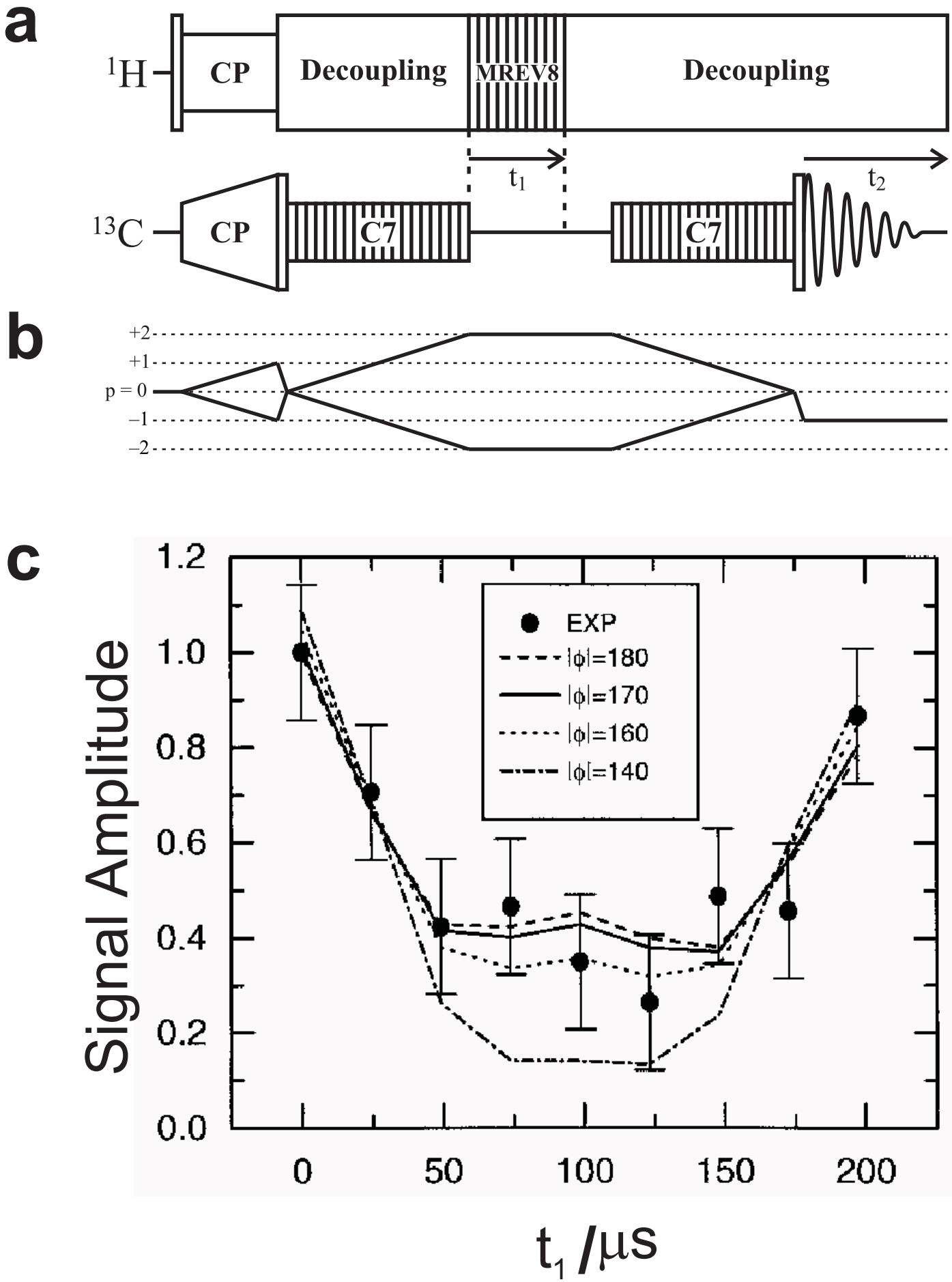
a
^{1}H
CP
Decoupling
MREV8
Decoupling
t_1
t_2
^{13}C
CP
C7
C7
b
+2
+1
p = 0
–1
–2
c
Signal Amplitude
1.2
1.0
0.8
0.6
0.4
0.2
0.0
EXP
|ϕ|=180
|ϕ|=170
|ϕ|=160
|ϕ|=140
0
50
100
150
200
t_1 /μs

Figure 14